Environmental Research 235 (2023) 116615

Contents lists available at ScienceDirect

Environmental Research

journal homepage: www.elsevier.com/locate/envres

Spatio-temporal compounding of connected extreme events: Projection and hotspot identification

Manikanta Velpuri, Jew Das *, N.V. Umamahesh

National Institute of Technology, Warangal, India

ARTICLE INFO

Handling Editor: Robert Letcher

Keywords:
CMIP6
Connected extremes
Hotspot
India
Spatio-temporal compounding

ABSTRACT

In general, the impact of two different connected extreme events is noticed on the same duration and spatial area. However, the connected extreme events can have footprint over different temporal and spatial scales. Thus, this article analyses the connected extreme events over India using the spatio-temporal compounding technique to understand the impact at different temporal and spatial scales. This approach is applied to analyse the historical and future connected extreme events. In the present study, coincident heat waves and droughts (Event C1), coincident heat waves and extreme precipitation (Event C2) are considered as connected extreme events. The future events are investigated using the suitable global climate models (GCMs) projections under three climate change scenarios (Shared Socioeconomic Pathways (SSP) 2–4.5, SSP3-7.0, and SSP5-8.5). The suitable GCMs are identified with the help of compromise programming. Subsequently, the hotspot regions are identified applying the Regional Climate Change Index (RCCI) method. The outcomes from the study suggest that with increasing temporal compounding, the mean duration of extreme events also increases. Highest increase in mean duration is observed for Event C1 over PI (Peninsular India), WCI (West Central India), and some parts of CNI (Central Northeast India) regions. The regions with high magnitude of duration have low magnitude of occurrence. The duration of Event C1 is likely to increase with respect to climate change scenarios and temporal compounding, especially in the PI region and some parts of WCI. However, there is insignificant change in the duration of Event C2. The PI region identified as the most vulnerable region followed by WCI and HR regions. The highest percentage of area under the emerging hotspot category is noticed under SSP5-8.5 climate change scenario.

1. Introduction

The weather and climate driven extreme events are the result of complex interaction between the physical processes across multiple spatial and temporal scales (Zscheischler et al., 2020). In most of the cases, these extreme conditions impose significant threat to the natural and human systems. Unlike the individual climate extreme (or hazard), the combination of number of climate extremes often lead to much adverse consequences (Das et al., 2022; Raymond et al., 2020; Zscheischler et al., 2018; Zscheischler and Seneviratne, 2017). The combination of different climate extremes, also named as connected extremes (Raymond et al., 2020)/correlated or complex extremes (Benestad and Haugen, 2007)/compound extreme (Zscheischler et al., 2020), is initially introduced by Intergovernmental Panel on Climate Change (IPCC) Special Report on Climate Extremes (SREX) in 2012 (Seneviratne et al., 2012). Such events are everywhere and can occur as a myriad of different combinations of weather and climate phenomena resulting in many different types of impacts. Zscheischler et al. (2020) outlined four different typology of compound extremes, namely preconditioned (e.g., heavy precipitation on saturated soil), multivariate (e.g., drought and heat wave at same time), temporally compound (e.g., temporal clustering of precipitation events), and spatially compound (e.g., spatially occurring extremes affecting overall global crop yield) to characterise the compound extreme events. In recent times, the compound extreme has evolved as thrust area of research in order to improve the assessment of societal and ecological impacts as well as to develop methodology for detection and attribution (Hendry et al., 2019; Moftakhari et al., 2017; Van Den Hurk et al., 2015; Wahl et al., 2015). In the present analysis, for rest of the paper "*compound extreme events*" are referred as "*connected extreme events*".

With this understanding, previous studies examined the impact of different connected extreme events on the past climate related natural hazards (Leonard et al., 2014). In addition, the future changeability of connected extreme events are studied across the globe (Das et al., 2022;

* Corresponding author.
E-mail address: jewdas05@gmail.com (J. Das).

https://doi.org/10.1016/j.envres.2023.116615
Received 11 April 2023; Received in revised form 21 June 2023; Accepted 9 July 2023
Available online 11 July 2023

Fischer and Knutti, 2013; Lu et al., 2018; Tencer et al., 2016; Weber et al., 2020). As an instructive example, heat wave is used to make the readers understand about the motive of the present study. To characterise the hazard related to the heat wave, the number of hot days (e.g., 90th or 95th percentile of maximum temperature) are examined in a sequential manner (e.g., minimum of consecutive 3 days). However, a short break of cooler days among the hot days segregates the heat wave extreme in terms of intensity and magnitude. In this sense, some studies adapt flexible heat wave definition which can incorporate the short break of cooler days within the event (Baldwin et al., 2019; Lau and Nath, 2012, 2014). In other word, the methodology tries to compound the temporally separated hot days into a single heat wave event instead of several events. It is worth mentioning that the similar approach can be opted for the other events such as extreme precipitation and droughts. However, there is a dearth in the applicability of temporal compounding in the case of connected extreme events.

As discussed earlier, the spatial and temporal scale of natural processes influence the single or connected natural hazards. The spatial and temporal scales denote the area and the duration over which the hazard occurs, respectively. Therefore, the spatial and temporal scales of occurrence of natural hazards incorporate many orders of magnitude and modulate the relationships between natural hazards (Leonard et al., 2014). In this regard, the spatiotemporal clustering of individual and connected extreme events would enable to identify the hotspot of different natural hazards (Barton et al., 2016). However, there is a scarcity of studies which examine the extreme events with respect to their spatial and temporal occurrence to understand the significant impacts of extreme hazards. The spatiotemporal compounding/clustering technique is a powerful technique to identify the scales of different natural hazards (Barton et al., 2016). It enables to extract the spatiotemporal characteristics of natural hazard clusters that would help in understanding the potential impacts and their interrelation with society (Tilloy et al., 2021).

The investigation of connected extreme events over the historical period helps in understanding the different characteristics of the events. However, it is prudent to analyse such connected events in future which would help in devising sustainable policy strategies to mitigate the future adverse conditions. Therefore, the outputs from the Global Climate Models (GCMs) are very useful in providing probable future trajectories under different climate change scenarios. However, past studies suggested that the uncertainty associated with different sources should be accounted while assessing the climate change impact in foreseen future (Das et al., 2018, 2020; Das and Umamahesh, 2017, 2018; Mujumdar and Ghosh, 2008). The uncertainty related to GCM projections stems from the parameterization, model structure, spatial resolution of GCM, and future emissions (Teng et al., 2012). Hence, it is necessary to examine different GCMs to confirm the extent to which they can reproduce the observed major variations in hydrometeorological variables. In the present study, the outputs from thirteen GCMs under Coupled Model Intercomparison Project 6 (CMIP6) experiment are used under three different Shared Socioeconomic Pathway (SSP) scenarios. To minimize the GCM uncertainty, the most suitable GCM at each grid point for different meteorological variables is evaluated using compromise programming. The details of the methodology are discussed in Section 2.

In the present study, spatiotemporal clustering of connected extreme events in India at various scales (from zero days to three days and from local to regional scale) during the historical and future periods is conducted. The spatiotemporal features of precipitation and temperature extremes are analysed. Both the precipitation and temperature extremes are considered as significant hazards in India (Das et al., 2022). For instance, the duration of extreme precipitation events affect the infrastructure failure, landslide, flood losses, etc (Mukherjee et al., 2018). Similarly, heatwave and drought conditions influence its impact on human health and society (Chand and Biradar, 2017; Mazdiyasni et al., 2017; Singh et al., 2021). In addition to the spatiotemporal clustering of connected extreme events, the identification of hotspot region in India under future climate change scenarios is performed. The research objectives addressed in the present study are as follows: (i) To understand the role of temporal and spatiotemporal clustering on the occurrence of connected extreme events; (ii) To identify the projected hotspot regions associated with the connected extreme events. To the best of the authors' knowledge, there are no studies that investigate the spatiotemporal compounding of connected extreme events in India to identify the future hotspots.

2. Materials and methods

2.1. Datasets

The observed daily meteorological datasets namely precipitation (Pr) and maximum temperature (Tmax) are obtained from India Meteorological Department (IMD) at a spatial grid resolution of 0.25° Lat x 0.25° Lon and 1° Lat x 1° Lon, respectively (Pai et al., 2014; Srivastava et al., 2009). The datasets can be downloaded from https://www.imdpune.gov.in/Clim_Pred_LRF_New/Grided_Data_Download.html. For the analysis, the Tmax dataset is regridded to the resolution of 0.25° Lat x 0.25° Lon using the bilinear interpolation technique. For future meteorological datasets, the outputs from GCMs under the newly developed CMIP6 (Eyring et al., 2016) experiment are used. The future datasets are obtained from thirteen different GCMs under SSP2-4.5, SSP3-7.0, and SSP5-8.5 scenarios. The list of GCMs is presented in Table S1 in the Supplementary Information. The datasets are bias-corrected using Empirical Quantile Mapping (EQM) and regridded at 0.25° Lat x 0.25° Lon over South Asia by Mishra et al. (2020) and can be downloaded from https://zenodo.org/record/3987736. In the present study, the meteorological datasets are extracted over 4641 grid points covering India. The details of the GCMs used are presented in Table S1 (refer to Supplementary Information). The period from 1977 to 2016 is considered as baseline period (T0). The future period is divided into two parts i.e., 2021–2060 (T1) and 2061–2100 (T2).

2.2. Methodology

The graphical representation of the adopted methodology is presented as a flow chart in Fig. 1. First, the extreme events such as heat waves, droughts, and extreme precipitation are extracted based on the chosen threshold at each grid point during the historical period. Next, the suitable GCM is found out using the compromising programming at each grid point for Pr and Tmax, separately. Using the historical threshold value, the future extreme events are computed for different climate change scenarios. The temporal and spatial clustering of extreme events is performed to obtain the spatio-temporal overlaps of extreme events. Subsequently, the connected heat wave-drought, and connected heat wave-extreme precipitation clusters are identified. Finally, the identification of hotspots related to the connected extreme events are identified under different climate change scenarios.

2.2.1. Statistical performance indicators

To measure the efficacy of GCMs simulations with respect to the observed data, three statistical performance indicators are used, namely, percentage bias (PBIAS), Nash-Sutcliffe efficiency (NSE), and skill score (SS). The PBIAS measures the over or under estimation of the simulated values as compared to the observed ones (Gupta et al., 1999). The optimal value of PBIAS is zero. The PBIAS can be computed using Eq. (1) as stated below.

$$PBIAS = \left[\frac{\sum_{i=1}^{n} \left(Y_i^{obs} - Y_i^{sim} \right)}{\sum_{i=1}^{n} Y_i^{obs}} \right] \times 100 \quad (1)$$

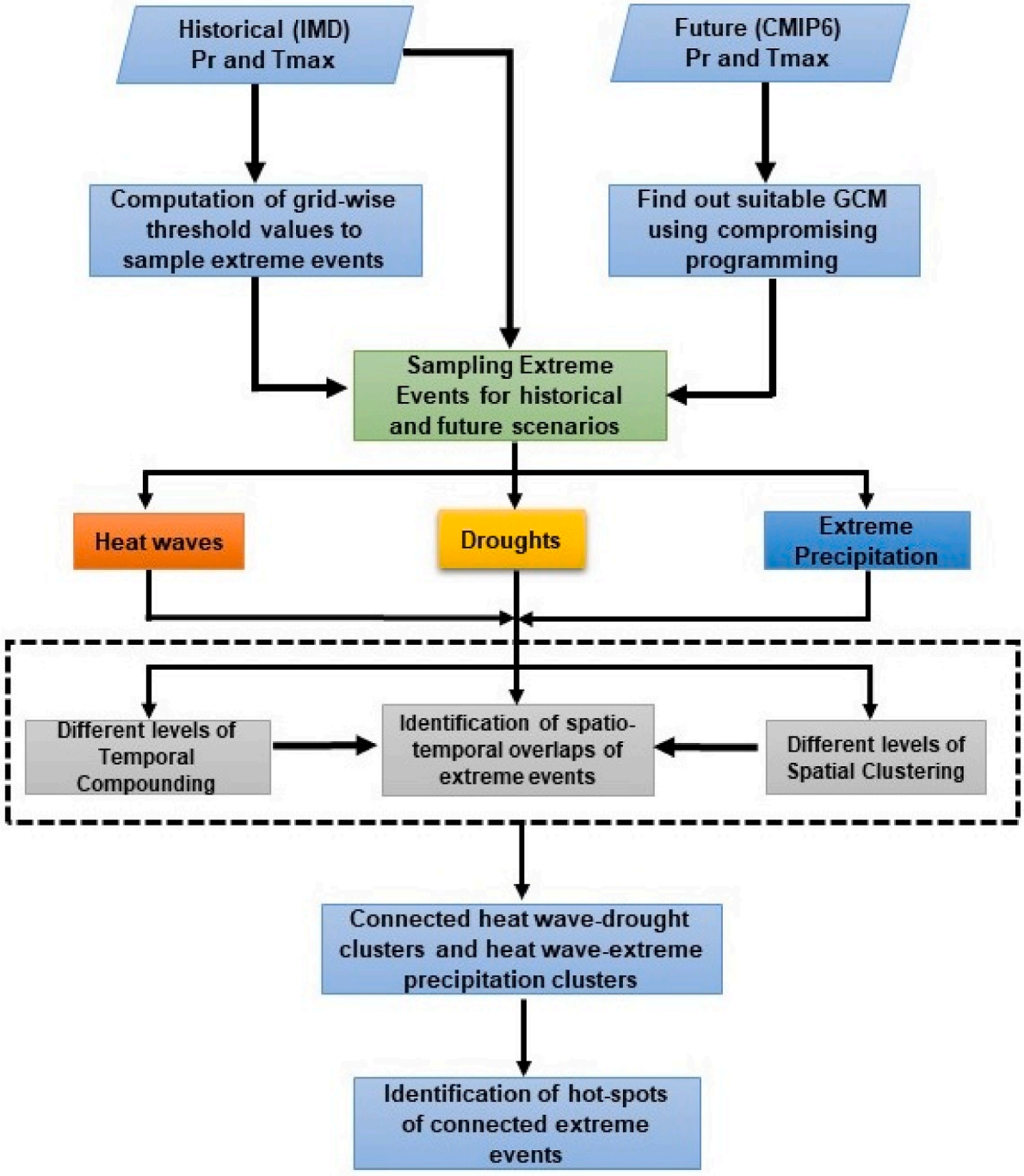

Fig. 1. Flowchart of the proposed methodology.

where Y_i^{obs} and Y_i^{sim} denote observed and simulated values at ith observation and n represents the total number of observations. Here, PBIAS is expressed as a percentage.

The NSE determines the relative magnitude of residual variance compared to the measured data variance (Nash and Sutcliffe, 1970) and can be computed as shown in Eq. (2).

$$NSE = \left[\frac{\sum_{i=1}^{n} \left(Y_i^{obs} - Y_i^{sim}\right)^2}{\sum_{i=1}^{n} \left(Y_i^{obs} - Y^{mean}\right)^2} \right] \quad (2)$$

The Y^{mean} is the mean of the observed data. The NSE ranges between -inf and one with NSE equal to one being the optimum value. Generally, values between zero and one are viewed as acceptable level of performance. However, the value $\leq$ zero is considered as unacceptable performance.

The SS measures the similarity between the probability density functions (PDF) of modelled and observed data and is expressed as follows:

$$SS = \sum_{i=1}^{nb} \min(f_{obs}, f_{sim}) \quad (3)$$

where f_{obs}, f_{sim} are the frequencies from the observed and modelled datasets and nb is the number bins chosen to compute the PDF. A bin size

of 1 mm is used for precipitation and 0.1° is used for temperature. The SS value of one suggests very good agreement between the simulated and observed frequencies.

2.2.2. Selection of GCM using compromise programming

Initially, the performance of historical simulations of GCMs at each grid is evaluated using the aforementioned statistical performance indicators. The weightage for each statistical indicator is computed using entropy method to find out the relative importance among the indicators (Raju and Kumar, 2014). The compromise programming is employed to rank the GCMs by aggregating the three statistical indicators. The distance (L_p) of a GCM from the available ideal set is defined in Eq. (4) and the GCM with minimum L_p value is selected as the best suitable GCM for the corresponding grid.

$$L_p(a) = \left[\sum_{j=1}^{J} w_j^p \left| g_j^* - g_j(a) \right|^p \right]^{\frac{1}{p}} \quad (4)$$

where j defines the statistical indicators, J is the total number of indicators; $L_p(a)$ is the L_p metric of GCM a for the chosen value of parameter p; g_j^* represents normalised ideal value of jth indicator; $g_j(a)$ defines the normalised value of jth indictor of GCM a; w_j is the weightage of jth indictor obtained from entropy method; p is one for linear and, two for squared Euclidean distance measure. Here, p is considered as two for squared Euclidean distance. Fig. 2 presents the grid count where a particular GCM has performed better in order to capture the historical precipitation and temperature time series. In case of temperature, NorESM2-LM, and EC-Earth3 models are found suitable for ~700 grid points individually followed by EC-Earth3-Veg and BCC-CSM2-MR climate models. The present outcomes are in line with the findings of Anil et al. (2021). Likewise, the GCMs, namely MPI-ESM1-2-LR, MRI-ESM2-0, and INM-CM5-0 are considered as top three performing GCMs and best suited for ~450 grid points individually.

In the performance evaluation of GCMs, precipitation and temperature simulations were assessed using percentage bias and skill score as evaluation metrics. The results, presented in Figs. S1 and S2, show that the percentage bias for precipitation ranges between −2% and 2% across most regions compared to IMD observations. The skill score values indicate a high agreement (0.91–0.99) between individual GCMs and IMD for precipitation. For maximum temperature simulations, Figs. S3 and S4 demonstrate a low percentage bias (−1%–2%) and high skill score, indicating good agreement with IMD observations. To compare the ability of GCMs in simulating compound extremes, plots were created for compound events (C1 and C2) along with IMD observations. The results indicate that GCMs capture the spatial variability of event C2 is aligning well with historical compound extremes from IMD observations. However, GCMs tend to underestimate the historical simulation of event C1. These findings provide insights into the performance of GCMs in simulating both individual climate variables and compound extremes, facilitating a comprehensive understanding of their ability to capture historical climate patterns.

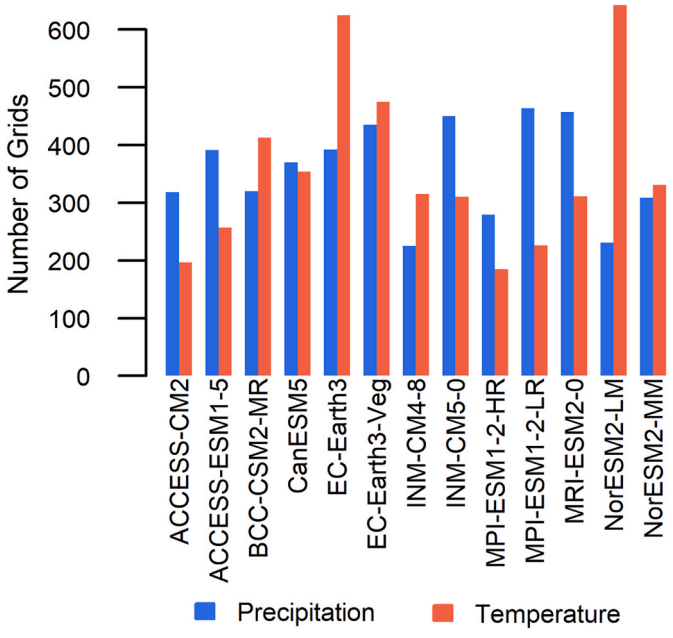

Fig. 2. Bar plot of different GCMs and their suitability over total number of grid points.

2.2.3. Defining the extreme events

In the present study, heat waves, droughts, and extreme precipitation are considered as extreme events. A period of three or more consecutive days with maximum temperature above the 95th percentile value during the baseline period is considered as heat wave (Das et al., 2022; Das and Umamahesh, 2021; Liu et al., 2017). In addition, the threshold is set to 25 °C if the 95th percentile is less than 25 °C (Weber et al., 2020). Likewise, the periods with precipitation less than 1 mm for five or more consecutive days are considered as drought. The duration with precipitation above the 95th percentile of the wet days (i.e., ≥1 mm precipitation) is referred as extreme precipitation. Considering the individual extreme events, the connected extreme events are proposed as the period when two extreme events coincide for one or more days and are called as coincident connected extreme. In the present study, coincident heat waves and droughts (C1), coincident heat waves and extreme precipitation (C2) are considered.

2.2.4. Temporal compounding of extreme events

In our study, we define precipitation and temperature extremes characterized by intermittent temporal breaks as temporally compound extreme events. When precipitation and temperature extremes occur in close proximity with short breaks of non-extreme events in between, they have the potential to compound together and result in escalated impacts that go beyond what is typically recognized by their respective standard definitions. This variable temporal structure, observed in extreme temperature and precipitation events leading to high mortality and floods, respectively. The graphical representation of the adopted framework (Baldwin et al., 2019) is depicted in Fig. 3. This figure provides a clear visualization of the temporal compounding of individual extreme events (Fig. 3(a)) as well as connected extreme events (Fig. 3 (b)). The red and blue dashed lines represent the thresholds above which an event is classified as extreme for temperature (heat wave) and precipitation (extreme precipitation), respectively. In the case of 1-day temporal compounding, even if there is a one-day gap between two individual extreme events, they are considered as a single extreme event. Similarly, for 2-day and 3-day temporal compounding, a maximum gap of two and three days, respectively, is allowed between individual extremes. To provide an example, let's consider a temperature threshold of 39.1 °C. If there is a heat wave event with temperatures exceeding the threshold on the first three days (39.4 °C, 39.3 °C, and 39.9 °C), followed by a non-extreme day with temperatures below the threshold on the fourth day, and then the temperature exceeds the threshold again on the fifth day, we consider it as a single event with 1-day temporal compounding. Fig. 3(a) illustrates the 1-day, 2-day, and 3-day compounding of heat waves, represented by grey, green, and blue colour boxes, respectively. Notably, when employing a 3-day temporal compounding, temporarily separated heat wave events are treated as a single event. Fig. 3(b) focuses solely on the 3-day temporal compounding of connected extreme events. The black dashed line within the figure indicates the common window where the 3-day compounding of each event is considered.

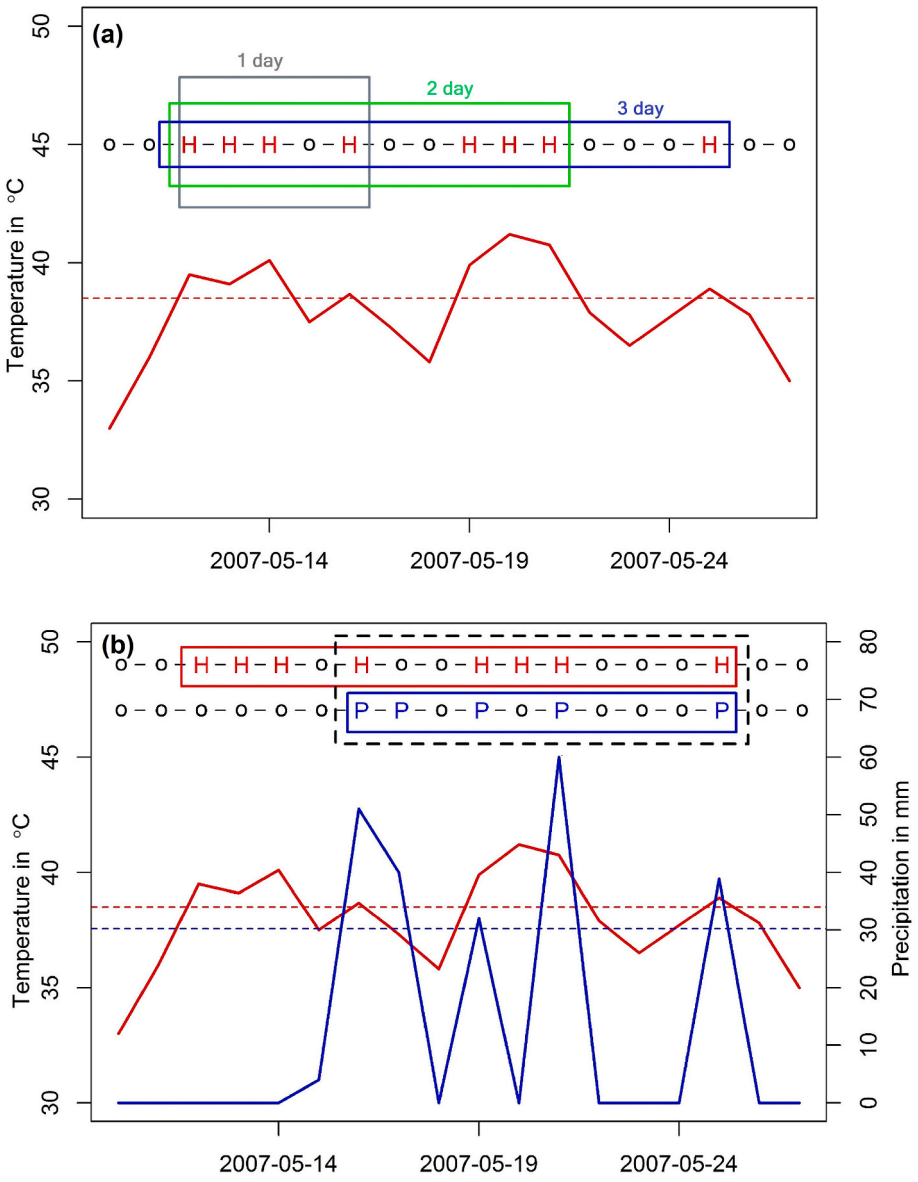

Fig. 3. (A) Graphical illustration of temporal compounding of individual extreme and (b) connected extreme.

2.2.5. Spatio-temporal compounding of extreme events

The spatial compounding enables to capture the extreme events occur simultaneously over a predefined spatial threshold. In order to perform the spatial clustering, the present study uses the connected component labelling algorithm (Falcão et al., 2004) where all the connected grids share the same label and treated as a single event (Nikumbh et al., 2019). The number of grids such as 16 (small-scale), 144 (medium-scale), and 400 (large-scale) are considered as spatial thresholds following the study by Nikumbh et al. (2019). Fig. 3 presents the spatio-temporal compounding of individual and connected extreme events for spatial compounding of 16 grids with 1-day temporal compounding and hence called as spatio-temporal compounding. It should be noted that the temporal compounding is performed at a particular grid point. However, the spatial compounding incorporates the nearby grids where an extreme event (or connected extreme events) is occurring simultaneously for different spatial thresholds. In Fig. 4, the spatial compounding is performed at each day up to n days for drought and heat wave events. Subsequently, the overlap portion of spatial compounding of heat wave and drought is demarcated as event C1 clusters. Similarly, spatio-temporal compounding is performed for all the spatial thresholds and 2-day, and 3-day temporal compounding.

2.2.6. Identification of future hotspots

A hotspot is defined as the geographical region which is highly vulnerable to the changes in present or future climate posing a severe threat to the human safety (Gu et al., 2014). Identification of these regions that experience accelerated climate change is important for risk assessment and adaptation strategies. Generally, these hotspots are defined based on the variations in different statistics (mean, variability and extremes) of projected changes in climate variables such as precipitation and temperature (Sherbinin, 2014). The mapping of climate change hotspots has been widely practiced by employing various indices such Regional Climate Change Index (RCCI) by Giorgi (2006), Climate Change Index (CCI) by Baettig et al. (2007), Standard Euclidean Distance (SED) by Williams et al. (2007), Squared Cord distance Dissimilarity coefficient (SCD) by Diffenbaugh et al. (2008). In this study, the hotspot regions are identified by adopting the methodology from Giorgi (2006). A Hotspot Index is defined based on two variables i.e., change in number of extreme events and change in mean duration of extreme events. Here, change indicates the percentage change in the variables

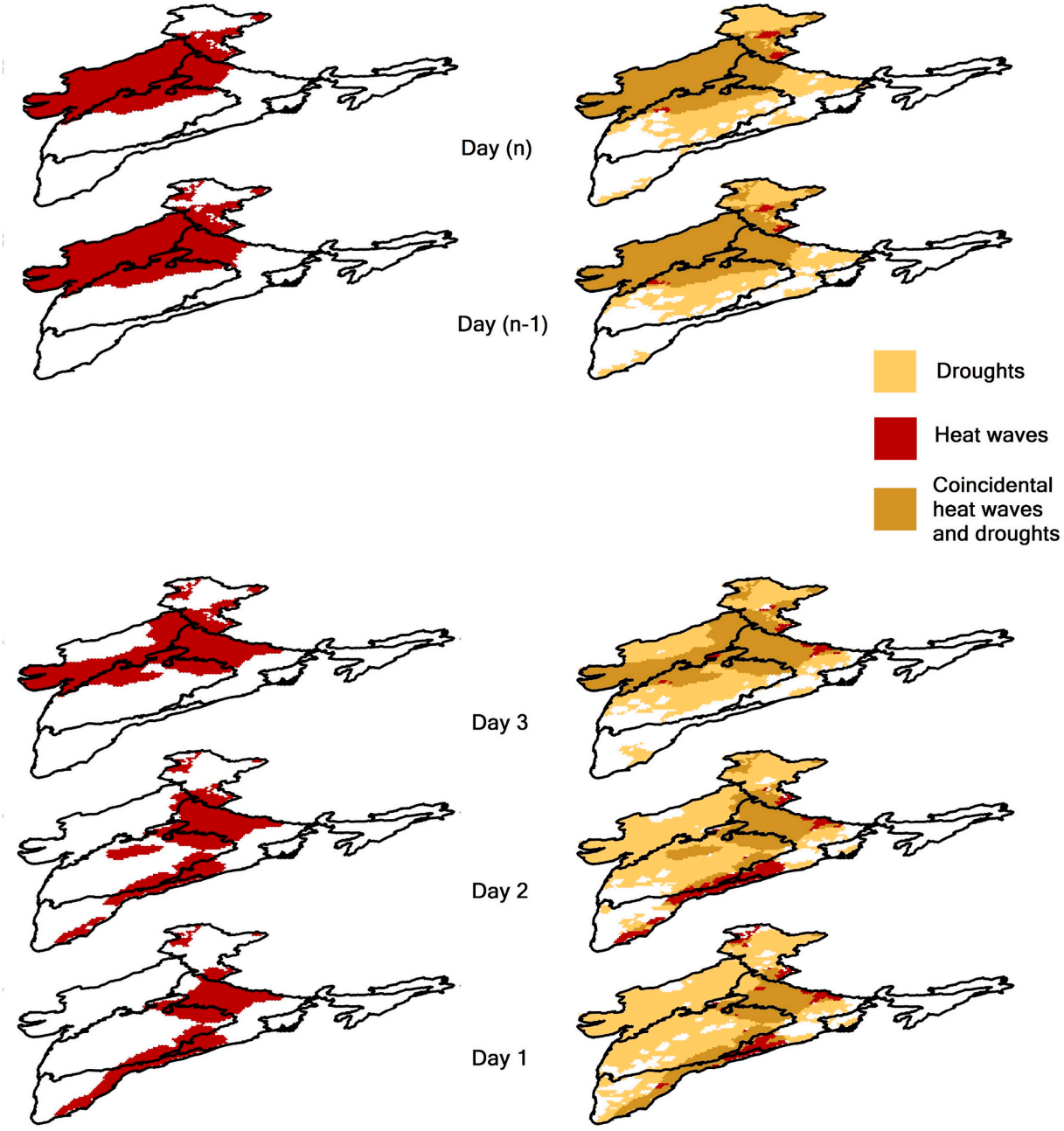

Fig. 4. Spatial compounding at each day up to n days for drought and heat wave events. The overlap portion of spatial compounding of heat wave and drought is demarcated as event C1 clusters.

obtained from future period (2021–2060 i.e., T1 and 2061–2100 i.e., T2) with respect to the baseline period (1977–2016). The Hotspot Index is defined as below.

$$Hotspot\ Index = [n(\Delta N) + n(\Delta D)]_{Event} \quad (5)$$

where n is an integer varying from 0 to 4 depending upon the percentage change in the future, and ΔN and ΔD represent the percentage change in the number of events and duration, respectively. The value of n is taken as 0,1,2 and 4 for the percentage changes of <5%, 5–10%, 10–20% and >20%, respectively. It is important to note that small changes below a certain threshold (<5%) do not contribute to the index ($n = 0$) and the value of n increases with respect to the percentage change of the variable (i.e., the factor n doubles from each category to the next). As an example, the location where both ΔN and ΔD of Event C1 is above 20%, the value of Hotspot Index is 8.

3. Results

In this section, the outcomes obtained from the spatio-temporal compounding of connected extremes during the historical and future projections under different climate change scenarios are presented. In addition, the identified possible future hotspot regions are discussed. The results are presented over six different zones of India (refer Fig. S7), namely Central Northeast India (CNI), Hilly Regions (HR), Northeast India (NEI), Northwest India (NWI), Peninsular India (PI), and West Central India (WCI).

3.1. Historical mean duration of extreme events for small-scale spatial compounding

Fig. 5 depicts the mean duration (i.e., mean of all events during

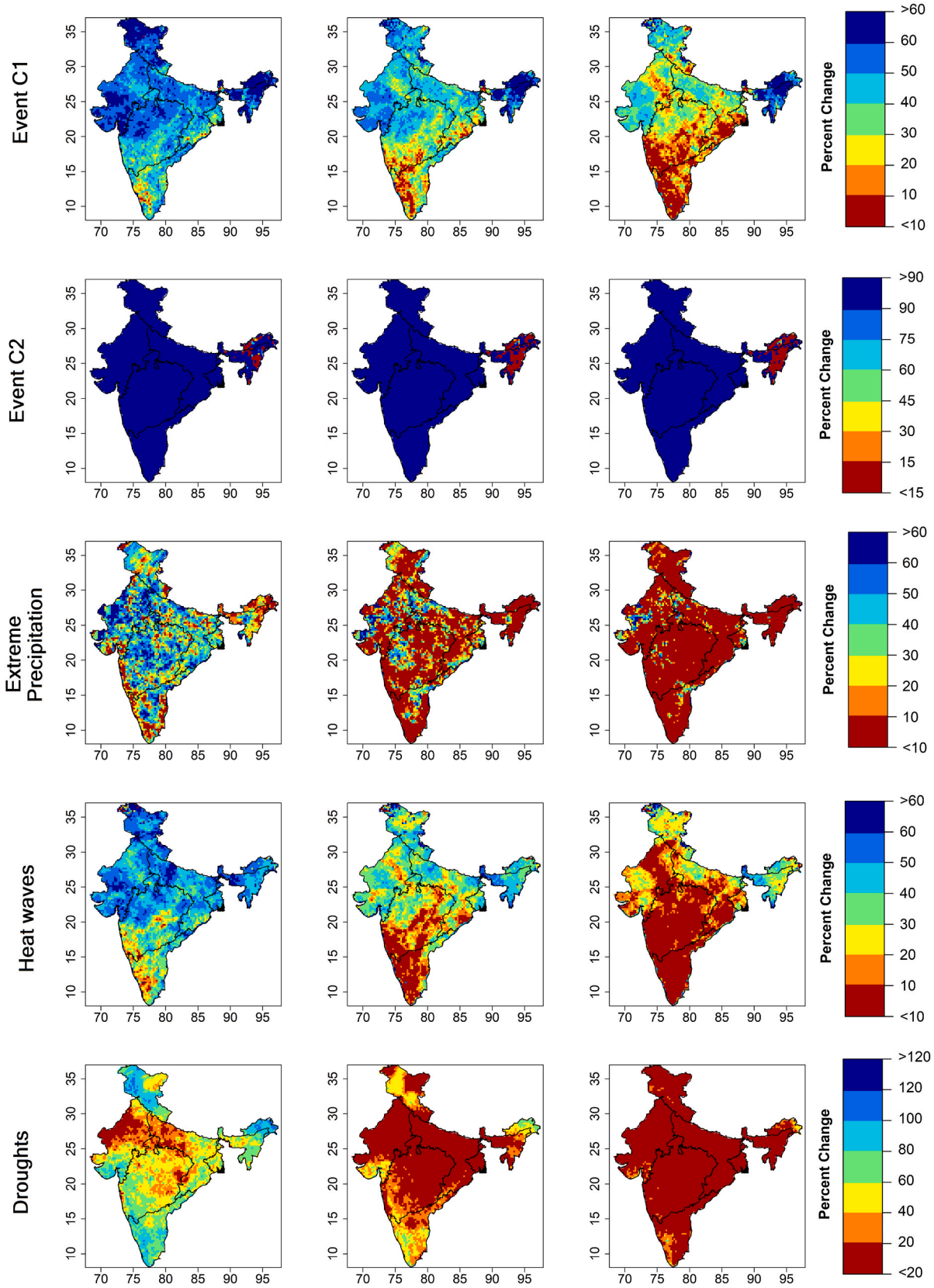

Fig. 5. The percentage change of mean duration (i.e., mean of all durations during 1977–2016) of extreme events in case of small-scale spatial compounding. The temporal compounding for 1-, 2-, and 3-days is presented (column-wise arrangement) in terms of percentage change with respect to the 0-day temporal compounding.

1977–2016) of extreme events in case of small-scale spatial compounding. In addition, the temporal compounding for 1-, 2-, and 3-days is presented (column-wise arrangement) in terms of percentage change with respect to the 0-day temporal compounding. In general, the percentage in the mean duration has increased from 1-day to 3-day temporal compounding of connected and individual extreme events. In case of event C1, the highest increase is observed over the PI, WCI, and some parts of the CNI regions. Over NEI, the percentage change in the mean duration has not varied significantly over different temporal compounding periods. For C2 events, the maximum change is noticed over NEI region. Except for NEI, no significant change in the mean duration of event C2 is observed over other regions even after the temporal compounding of 1-, 2-, and 3-days. In case of individual extreme event like extreme precipitation, the change in the mean duration is more significant at 2- and 3-days temporal compounding. At 3-day temporal compounding, the highest percentage change with respect to 0-day compounding is noticed over some parts in the NEI, and PI regions. The mean duration of heat wave event has increased from 1- to 3- days temporal compounding over most of the parts of PI and WCI regions. In contrast, unlike other individual extreme events, the mean duration of drought events has increased over NWI, CNI, and some parts of the WCI.

3.2. Historical mean duration of extreme events for medium- and large-scale spatial compounding

The mean duration of different extreme events for medium- and large-scale spatial compounding are presented in Fig. S8 and Fig. S9 (in the Supplementary Information), respectively. From Fig. S8, it can be observed that the historical change in case of C1 event is not significantly different from small-scale spatial compounding for 1-, 2-, and 3-days temporal compounding. However, the area with high percentage change with respect to historical period has decreased in case of large-scale spatial compounding (Fig. S9). The event C2 has no effect due to the different scale spatial and temporal compounding across India. In case of extreme precipitation, the percentage change of mean duration has decreased while comparing with various spatial compounding approaches. A similar kind of pattern is observed for heat wave events. Conversely, an increment (decrement) in the areal spread of maximum change in the mean duration of drought is noticed under large-scale spatial compounding as compared to small- and medium-scale spatial compounding over CNI (HR) region.

3.3. Historical occurrence of extreme events for small-, medium- and large-scale spatial compounding

The percentage change in the occurrence of different extreme events with respect to 0-day temporal compounding for small-, medium- and large-scale spatial compounding are presented in Fig. S10, Fig. S11, and Fig. S12, respectively (refer to Supplementary information). In general, it is found that the regions with high magnitude (i.e., percentage change is significantly more) of duration are associated with the low magnitude of occurrence (i.e., percentage change is significantly less). From Fig. S10, it is found that the number of extreme events (except for Event C2) is getting less with increasing duration of temporal compounding. In spite of the temporal compounding, some parts in the HR and NEI have no significant variations in Event C1. In the case of heat wave, the larger variability due to the temporal compounding is noticed mostly over PI and WCI regions. Similarly, the variation in the number of events is highest over NWI and CNI regions in case of droughts. It can be noted from Fig. S11 that significant decrease in the occurrence of events is observed over most of the parts of WCI in Event C1, over PI and NEI in extreme precipitation, over PI, and WCI in heat waves, and over NWI, and CNI in case of droughts. The outcomes from the large-scale spatial compounding (Fig. S12) reveal that the highest decrease in the occurrences due to temporal compounding is noticed over NEI for Event C1. With increase in the temporal compounding, the areal extent of percentage decrease in the events C1, extreme precipitation, heat waves, and droughts is computed to be increased. The decrease in the number of events is observed with increasing the scale of spatial compounding in the cases of event C1 (over NEI region) and extreme precipitation. Conversely, the occurrence of heat wave events is evaluated to be increased (i.e., higher negative value to lower negative value) with spatial compounding. In the case of droughts, the region is likely to be shifted from small-to large-scale spatial compounding. For instance, the highest percentage decrease in the droughts is observed over the NWI region. However, with spatial compounding it is found that the region with highest percentage decrease is noticed over CNI.

3.4. Future occurrence of connected extremes under different spatio-temporal compounding

This section delivers the outcomes related to the future projection of connected extreme (Event C1) with various temporal and spatial compounding criteria. It should be noted that only the connected extremes are analysed for future projections. The future changes of occurrence are evaluated during T1 and T2 periods in terms of percentage change with respect to the historical observations. Fig. 6 depicts the 1-day temporal compounding of Event C1 for all the spatial scales. Figures from 6(a)-6(f), 6(g)-6(l), and 6(m)-6(r) present small-, medium-, and large-scale spatial compounding for different climate change scenarios, respectively. While comparing the time period (T1 and T2), it is noticed that the percentage change is higher in case of T2 period as compared to T1 period under all the spatial compounding criteria and climate change scenarios. In the case of projection scenarios, it is observed that the percentage change is anticipated to increase with future scenarios (i.e., from SSP2-4.5 to SSP5-8.5) during T2 period. With increase in the spatial compounding, the number of Event C1 is projected to decrease over HR, and some portions of CNI and NEI regions. Conversely, an increase in the number of C1 events is expected over most parts of PI and some parts of WCI region. In case of T1 period, the number of C1 event is likely to decrease with respect to increase in spatial scales across most parts of India. However, the rate of decrement over HR, and some portions of CNI and NEI regions is very high as compared to the rate of decrement in other regions. The west coast portions in PI and WCI and some portions of NEI are likely to experience higher number of Event C1 in both T1 and T2 periods (except for large-scale spatial compounding during T1 period).

Similarly, the spatial distribution of percentage change in Event C1 for 2-day and 3-day temporal compounding for different spatial scales are plotted in Figs. S13 and S14, respectively. A similar kind of future pattern related to climate change scenarios and duration (T1 and T2) is observed as in case of 1-day temporal compounding. It is noticed that the region with less occurrence of C1 event (mostly HR region) during 1-day temporal compounding is expected to face more frequent (i.e., shifting from negative percentage change towards positive percentage change) C1 event under 2-day and 3-day temporal compounding for medium-scale spatial compounding. However, the region with high occurrence of C1 event (mostly WCI region) during 1-day temporal compounding is expected to face less C1 event under 2-day and 3-day temporal compounding for all spatial compounding. It is worth mentioning that the regions with negative percentage change in case of 1-day temporal compounding have not undergone significant change under 2-day and 3-day temporal compounding for small- and large-scale spatial compounding. Accounting all the temporal and spatial compounding, the most affected regions due to Event C1 are located over NEI, east coast of CNI, and most parts of PI region.

The spatial distribution of percentage change in Event C2 for 1-day, 2-day and 3-day temporal compounding for different spatial scales are plotted in Figs. S15, S16, and S17, respectively. It can be noted from the figures that the percentage change in the Event C2 has insignificant affect due to the temporal and spatial compounding. Some parts of the HR region and NEI region are expected to experience the consequences

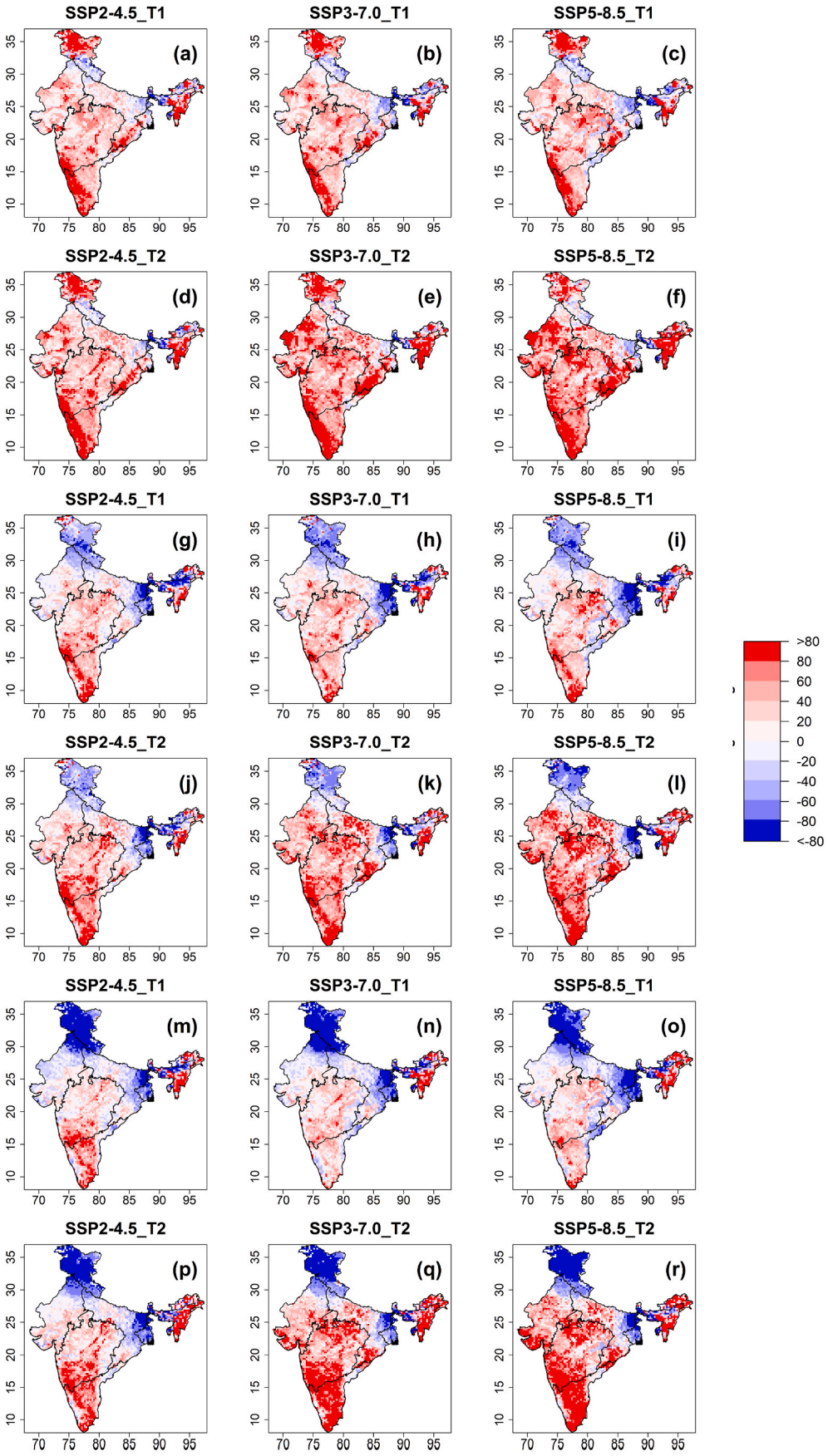

Fig. 6. 1-day temporal compounding of Event C1 occurrence for all the spatial scales. Figures from (a)–(f), (g)–(l), and (m)–(r) present small-, medium-, and large-scale spatial compounding for different climate change scenarios, respectively.

of Event C2.

3.5. Future duration of connected extremes under different spatio-temporal compounding

Fig. 7 presents the change in the future duration of Event C1 for 1-day temporal compounding under three different spatial compounding criteria. Like Fig. 6, the spatial scale compounding criteria are divided into groups. Figures from 7(a)-7(f), 7(g)-7(l), and 7(m)-7(r) present small-, medium-, and large-scale spatial compounding for different climate change scenarios, respectively. It is clearly evident that there is an increase in the duration of Event 1 under T2 period as compared to T1 period. Similarly, the duration is projected to increase with respect to the climate change scenario. In the cases of medium- and large-scale compounding the increase in the duration of Event C1 is noticed mostly over PI region and some parts of WCI region. However, a decrease in the duration is projected over the remaining regions of India. The areal coverage of percentage of increase in the duration is more for small-scale compounding as compared to the medium- and large-scale compounding. The areal coverage includes most parts of PI and some parts of WCI, NWI, CNI, and HR regions.

The percentage change of duration for 2-day and 3-day temporal compounding is presented in Figs. S18 and S19, respectively. From the figures, it can be noted that a similar observation is noticed as in case of 1-day temporal compounding while comparing the outcomes with respect to duration and climate change scenarios. In general, the spatial extent of percentage change in the duration of Event C1 is expected to increase with respect to temporal compounding. In other words, areal extent is projected to be more in the case of 3-day temporal compounding while comparing with 1-day and 2-day temporal compounding. In addition, the areal extent is more for small-scale spatial compounding as compared to medium- and large-scale spatial compounding. In the case of Event C2 (Figs. S20, S21, and S22), insignificant change in the duration of observed over most parts of India (except some parts of HR and NEI regions) under different spatial and temporal compounding.

3.6. Identification of hotspot under projected climate change

The spatial distribution of hotspot regions for 1-day temporal compounding is plotted in Fig. 8 for different spatial compounding. Under the first hotspot drought category (i.e., 0–2), it is observed that with increasing spatial scale the percentage area under this category is likely to increase over all the regions under different climate change scenarios. The percentage of area under 0–2 hotspot category during T2 period is projected to decrease as compared to T1 period. Unlike the hotspot category (i.e., 0–2), with increasing spatial scale the percentage area under this 2-4, 4–6 and 6–8 categories is likely to decrease over all the regions under different climate change scenarios. Under the emerging hotspot category (i.e., 6–8) is projected over the regions of NWI, PI, and WCI. The percentage of area under this hotspot category during T2 period is projected to increase as compared to T1 period. The highest percentage of area under the 6–8 category is noticed under SSP5-8.5 climate change scenario.

The hotspot characterization with respect to 2-day and 3-day temporal compounding is presented in Figs. S23 and S24, respectively. An overview of all the temporal compounding reveals that the emerging hotspot category is likely to increase with increase in temporal compounding. The percentage of area under 6–8 category is highest in case of small-scale spatial compounding as compared to the medium- and large-scale compounding. With increase in the climate change emission scenarios, the area under emerging drought category is likely to increase in most of the cases during T2 period as compared to T1 period. The PI region is identified as most vulnerable region followed by WCI and NWI regions under the category of emerging hotspot in case of 2-day temporal compounding. The findings from 3-day temporal compounding are similar to the 2-day compounding with most vulnerable regions identified over PI, WCI, and CNI.

4. Discussion

In the present study, the connected extreme hazard events over India and their overlap in space and time has been examined during historical and future projections under different climate scenarios. GCMs are the most widely used tools for projecting future climate change. Differences in model design, parameterization, and input data can result in significant variations in model output (Hawkins and Sutton, 2012). Therefore, it is essential to carefully evaluate GCMs before selecting them for use in studies of future climate extremes. One approach to selecting and ranking GCMs is to evaluate their ability to simulate present-day climate. Several studies have shown that GCMs that perform well in simulating current climate conditions tend to produce more accurate projections of future climate change (Knutti et al., 2017). In this study, compromise programming is used to rank the GCMs due to the following reasons: (i) It allows for the selection of GCMs that perform well on a range of evaluation criteria, rather than just selecting one GCM that performs best on a single criterion (Pradhan et al., 2021); (ii) additionally, this allows to incorporate their own evaluation criteria and weighting schemes, ensuring that the rankings are tailored to the specific research goals (Srinivasa Raju et al., 2017).

A comprehensive understanding of compound hazards (here, connected extremes) requires analyzing their characteristics across both spatial and temporal dimensions. This approach offers a more complete view of the complex interrelationships among the hazards involved and can provide valuable insights into the nature of compound hazards occurrences (Sadegh et al., 2018). The findings of this study reveal that the mean duration of extreme events has generally increased with increasing temporal compounding, and this change varies across different types of extreme events and regions. In terms of small-scale spatial compounding, the highest increase in the mean duration of Event C1 is observed over the Peninsular India (PI), West Central India (WCI), and some parts of the Central Northeast India (CNI) regions. The results are found to be in agreement with the findings of Yu et al. (2022), Muthuvel and Mahesha (2021), and Sharma and Mujumdar (2017). Some parts of the HR region and NEI region are expected to experience the consequences of Event C2, and this result is consistent with the findings of Das et al. (2022). High surface temperatures and sensible heat flux, which enhance the convective available potential energy and increase the likelihood of heavy precipitation events, are usually linked to the occurrence of extreme heat events (Ning et al., 2022). However, individual extreme precipitation events show a significant change in mean duration at 2- and 3-day temporal compounding, with the highest percentage change observed in some parts of the NEI and PI regions. The increased frequency of extreme precipitation across India can be attributed to a combination of changing climate and increased anthropogenic activities (Sarkar and Maity, 2022). Suman and Maity (2020) discovered a non-uniform pattern of increasing air temperature and precipitation water over South Asia. The projections show that air temperature over the Tibetan Plateau and the Himalayas is expected to rise significantly, which could enhance the Indian Ocean Dipole and create favourable conditions for the Indian Summer Monsoon (ISM). The rise in air temperature in India could lead to an increase in atmospheric moisture-holding capacity, resulting in more extreme precipitation events over the area. During monsoon months, the eastward moisture flux over the Indian Ocean and Arabian sea region intensifies, resulting in more moisture-laden wind entering south India through the western coast and enhancing precipitation extremes in the southern part of the country. The Western Ghats mountain range on the western coast of India leads to more frequent extreme precipitation events occurring on the windward side (Goswami et al., 2006). However, further analysis is required to explain the zone-specific projections of precipitation extremes based on different variables such as air temperature, precipitable

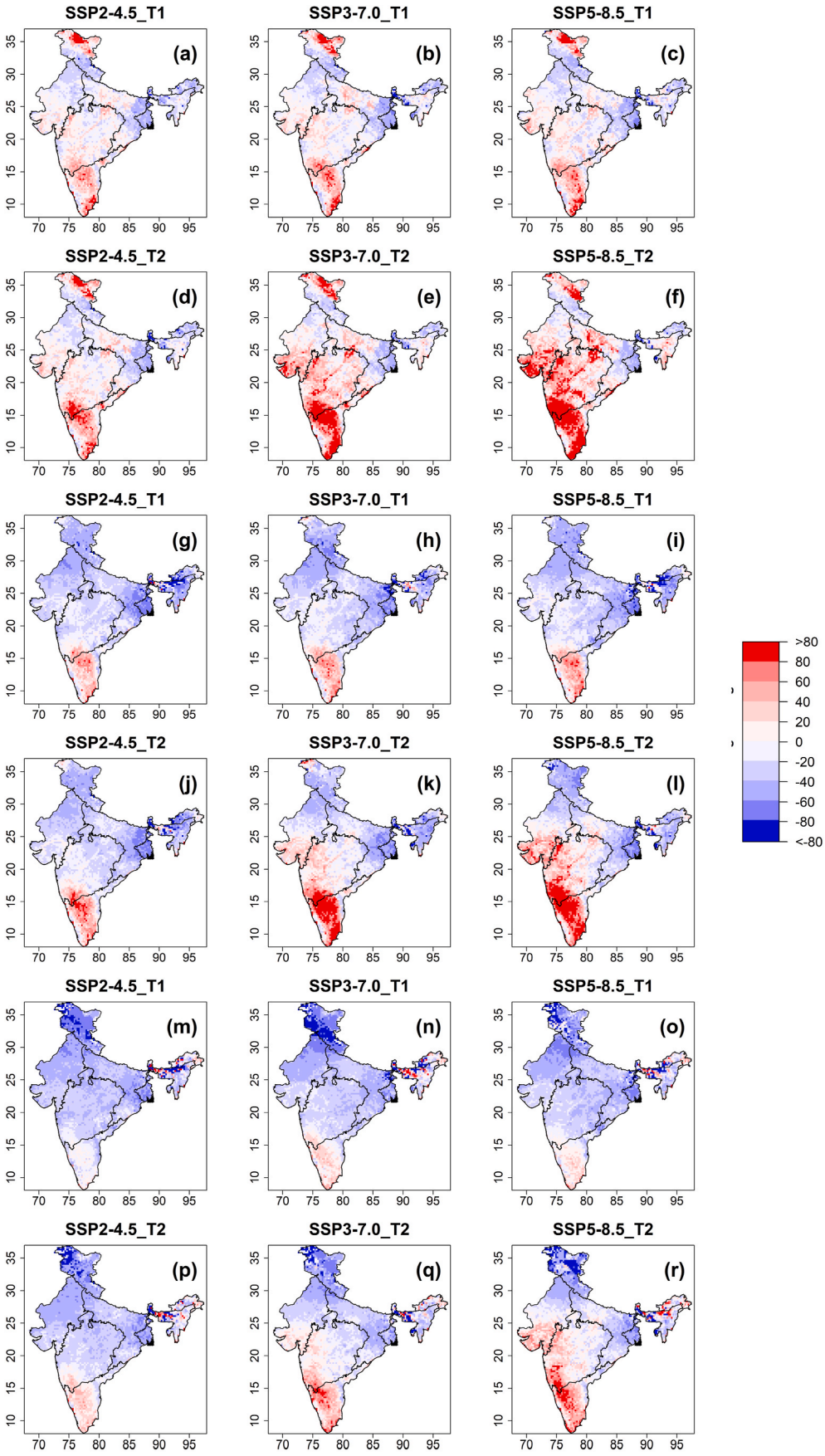

Fig. 7. 1-day temporal compounding of Event C1 duration for all the spatial scales. Figures from (a)–(f), (g)–(l), and (m)–(r) present small-, medium-, and large-scale spatial compounding for different climate change scenarios, respectively.

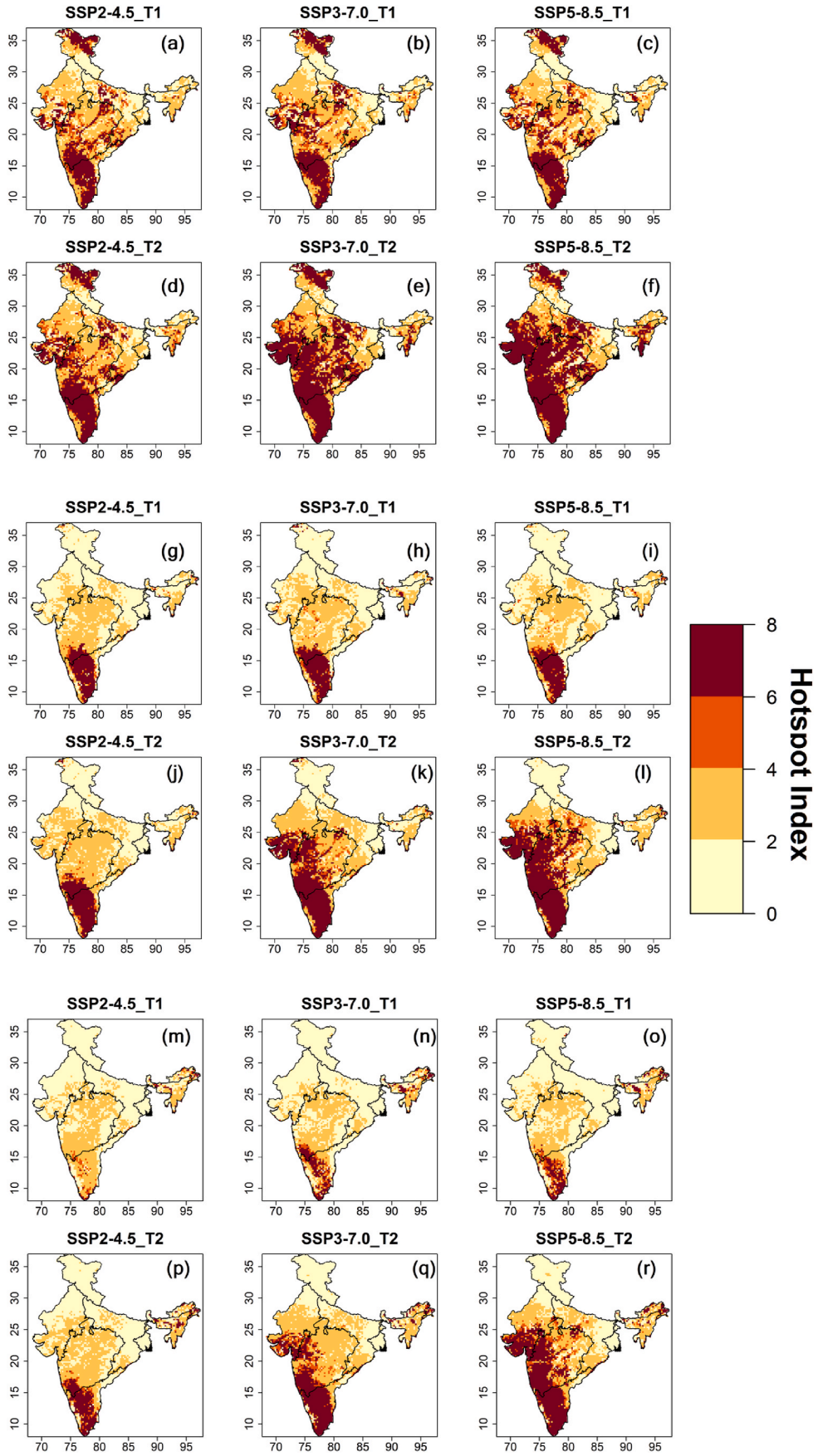

Fig. 8. Spatial distribution of hotspot regions for 1-day temporal compounding. Figures from (a)–(f), (g)–(l), and (m)–(r) present small-, medium-, and large-scale spatial compounding for different climate change scenarios, respectively.

water, moisture flux, and convergence.

The results of the study suggest that temporal clustering has a significant impact on the duration of extreme events. If the percentage increase in mean duration compared to no temporal clustering is high, it implies that those regions are more vulnerable to such extreme events within a shorter period. The outcomes indicate that in small-scale spatial events, the mean duration of Event C1 exhibits a substantial increase (>60%) at PI, some parts of WCI, and CNI, particularly for 3-day temporal clustering, and comparable trends are observed for medium and large-scale events. Additionally, for Event C2, the mean duration shows an increasing trend at NEI with higher levels of temporal clustering. Concerning individual extreme precipitation, the mean duration increment at 3-day temporal clustering is significant at NEI and the eastern coast exposed to the Bay of Bengal, which is a warm and shallow water body favourable for the formation of tropical cyclones (Vishwakarma and Pattnaik, 2022). These cyclones bring about heavy rainfall to the eastern coast of India, especially during the monsoon season. Furthermore, the mean duration of heatwave events tends to increase with temporal clustering, primarily in parts of PI and WCI, while the mean duration of drought events is significantly high at NWI, CNI, and parts of WCI with higher levels of temporal clustering.

The emerging hotspot category (6–8) is projected to increase with increasing temporal compounding and is highest under the SSP5-8.5 climate change scenario. The PI region is identified as the most vulnerable region, followed by WCI and HR regions under the emerging hotspot category for 2-day and 3-day temporal compounding. The study also indicates that the area under the emerging drought category is likely to increase during T2 period as compared to T1 period under different climate change emission scenarios. The lack of previous studies on the hotspots of spatio-temporal compound extremes in India makes it difficult to draw comparisons with the results of this study. However, the current study's results are consistent with the identified hotspots in the literature for single extreme events. Narula et al. (2018) used a temperature-change index to identify hotspots clustering over the north-central and eastern-coastal parts of India, as well as some grids on its western borders. Similarly, Saha and Sateesh (2022) identified extreme precipitation hotspots in India at the western coast and Northeastern India.

The present analysis, however, has some limitations that includes subjectivity in definition of the threshold for pruning of extreme events in space and time. The subjectivity in the threshold translates into the identified hotspots, spatial and temporal clusters of extreme events, and the frequency and duration of extreme events. The gridded datasets often underestimate the frequency and intensity of extremes, particularly for precipitation extremes due to its high spatial variability with the complexity of the terrain (Kandlikar et al., 2005; Raymond et al., 2020). Hence, station-based daily meteorological data should be used in analysis of compound extremes, as they preserve the extreme events. The ranking procedure used to assess GCM performance introduces uncertainties due to subjective selection of evaluation metrics, Multi-Criteria Decision Making, and weight allocation, limiting the study's conclusions (Anil et al., 2021). Additionally, reliance on climate model simulations for projected climate extremes poses challenges due to the rarity of extreme events. Although global simulations of standard resolution provide valuable global statistical information at a lower computational cost, they may have limitations in regions with steep terrain, where high-resolution regional models are more suitable. Despite efforts to account for model deficiencies, natural variability, and feedback mechanisms, uncertainties persist in physical processes and model simulations.

Incorporating local land-air interactions is crucial for a comprehensive analysis of extreme events' impacts on vegetation and land cover. These interactions mediate ecosystem responses to compound extremes, influencing the magnitude and spatial patterns of vegetation stress, composition changes, and land cover alterations. Extreme events such as heat waves, droughts, and other connected events can have significant impacts on vegetation and land cover. These impacts include vegetation stress, changes in vegetation composition, land cover changes, and disruptions to ecosystem services (Allen et al., 2010). Heat waves and droughts can lead to water stress on vegetation, affecting growth and productivity. Competitive dynamics among plant species can be altered, leading to shifts in vegetation composition (D'Odorico et al., 2013). Changes in land cover patterns can occur due to droughts, including the drying of water bodies and increased risks of wildfires. Conversely, intense rainfall events can cause flooding and erosion. These changes in vegetation and land cover can have far-reaching effects on ecosystem services, influencing climate regulation, biodiversity, wildlife habitat, and resource availability. By considering local land-air interactions, we capture the complexity and heterogeneity of ecological responses, enhancing the robustness and applicability of our study findings.

Overall, the results highlight the spatial and temporal variability in the duration and occurrence of extreme events across different regions of India. The findings have important implications for climate change adaptation and mitigation strategies, as they suggest that different regions may experience varying levels of exposure and vulnerability to extreme events under different climate change scenarios. For example, the results suggest that the PI and WCI regions may be particularly vulnerable to heat wave events, while the NWI region may be more susceptible to droughts.

5. Conclusions

The present study adopted temporal and spatial clustering of connected extreme events to provide valuable insights into the characterization of extreme events. Subsequently, potential hotspots of different extreme events were identified to understand the spatial and temporal extent of compound hazards. The following conclusions are drawn from the findings of the study.

- The percentage change in the mean duration of extreme events generally increases with increasing temporal compounding during historical period. The highest increase in mean duration is observed for event C1 over PI, WCI, and some parts of CNI regions, while event C2 has no significant change in mean duration across India.
- The mean duration of extreme precipitation and heat wave events also increases with increasing temporal compounding, while the mean duration of drought event decreases in NWI, CNI, and some parts of WCI regions during historical period.
- The regions with high magnitude of duration have low magnitude of occurrence. The occurrence of extreme events generally decreases with increasing temporal compounding and spatial scale, except for heat wave events, which increase with spatial compounding.
- The duration of Event C1 is increasing with respect to climate change scenarios and temporal compounding, especially in the PI region and some parts of WCI. The areal coverage of percentage of increase in duration is more for small-scale compounding. However, there is insignificant change in the duration of Event C2.
- When comparing T1 and T2 time periods across all spatial compounding criteria and climate change scenarios, a higher percentage change was observed during T2. Furthermore, it is expected that the percentage change will increase in future projection scenarios (from SSP2-4.5 to SSP5-8.5) during the T2 period.
- Hotspot characterization revealed an increase in the emerging hotspot category with increase in temporal compounding, with the PI region identified as the most vulnerable region followed by WCI and HR regions. The highest percentage of area under the 6–8 category is noticed under SSP5-8.5 climate change scenario.

The analysis offers important insights for climate risk assessment on the spatio-temporal compound extreme events in India. These findings assist in the development of region-specific adaptation and mitigation policies and strategies aimed at reducing the impacts of connected

extreme events on vulnerable populations and ecosystems.

Credit author statement

Manikanta Velpuri: Conceptualization, Methodology, Writing – original draft, Jew Das: Methodology, Investigation, Writing – original draft, N V Umamahesh: Visualization, Investigation, Supervision, Writing- Reviewing and Editing.

Declaration of competing interest

The authors declare that they have no known competing financial interests or personal relationships that could have appeared to influence the work reported in this paper.

Data availability

Data will be made available on request.

Appendix A. Supplementary data

Supplementary data to this article can be found online at https://doi.org/10.1016/j.envres.2023.116615.

References

Allen, C.D., Macalady, A.K., Chenchouni, H., Bachelet, D., McDowell, N., Vennetier, M., Kitzberger, T., Rigling, A., Breshears, D.D., Hogg, E.H., Ted), Gonzalez, P., Fensham, R., Zhang, Z., Castro, J., Demidova, N., Lim, J.-H., Allard, G., Running, S. W., Semerci, A., Cobb, N., 2010. A global overview of drought and heat-induced tree mortality reveals emerging climate change risks for forests. For. Ecol. Manage. 259, 660–684.

Anil, S., Manikanta, V., Pallakury, A.R., 2021. Unravelling the influence of subjectivity on ranking of CMIP6 based climate models: a case study. Int. J. Climatol. https://doi.org/10.1002/joc.7164.

Baettig, M.B., Wild, M., Imboden, D.M., 2007. A climate change index: where climate change may be most prominent in the 21st century. Geophys. Res. Lett. 34 https://doi.org/10.1029/2006GL028159.

Baldwin, J.W., Dessy, J.B., Vecchi, G.A., Oppenheimer, M., 2019. Temporally compound heat wave events and global warming: an emerging hazard. Earth's Future 7, 411–427. https://doi.org/10.1029/2018EF000989.

Barton, Y., Giannakaki, P., von Waldow, H., Chevalier, C., Pfahl, S., Martius, O., 2016. Clustering of regional-scale extreme precipitation events in southern Switzerland. Mon. Weather Rev. 144, 347–369. https://doi.org/10.1175/MWR-D-15-0205.1.

Benestad, R.E., Haugen, J.E., 2007. On complex extremes: flood hazards and combined high spring-time precipitation and temperature in Norway. Clim. Change 85, 381–406. https://doi.org/10.1007/s10584-007-9263-2.

Chand, K., Biradar, N., 2017. Socio-economic impacts of drought in India. In: Drought Mitig. Manag. Sci. Publ., New Delhi, pp. 245–263.

D'Odorico, P., Bhattachan, A., Davis, K.F., Ravi, S., Runyan, C.W., 2013. Global desertification: drivers and feedbacks. Adv. Water Resour. 51, 326–344. https://doi.org/10.1016/j.advwatres.2012.01.013.

Das, J., Manikanta, V., Umamahesh, N.V., 2022. Population exposure to compound extreme events in India under different emission and population scenarios. Sci. Total Environ. 806 https://doi.org/10.1016/j.scitotenv.2021.150424.

Das, J., Poonia, V., Jha, S., Goyal, M.K., 2020. Understanding the climate change impact on crop yield over Eastern Himalayan Region: ascertaining GCM and scenario uncertainty. Theor. Appl. Climatol. 142, 467–482. https://doi.org/10.1007/s00704-020-03332-y.

Das, J., Treesa, A., Umamahesh, N.V., 2018. Modelling impacts of climate change on a river basin: analysis of uncertainty using REA & possibilistic approach. Water resour. Manag. https://doi.org/10.1007/s11269-018-2046-x.

Das, J., Umamahesh, N.V., 2021. Heat wave magnitude over India under changing climate: projections from CMIP5 and CMIP6 experiments. Int. J. Climatol. joc. 7246 https://doi.org/10.1002/joc.7246.

Das, J., Umamahesh, N.V., 2018. Assessment of uncertainty in estimating future flood return levels under climate change. Nat. Hazards 1–16. https://doi.org/10.1007/s11069-018-3291-2.

Das, J., Umamahesh, N.V., 2017. Uncertainty and nonstationarity in streamflow extremes under climate change scenarios over a river basin. J. Hydrol. Eng. 22, 04017042 https://doi.org/10.1061/(asce)he.1943-5584.0001571.

Diffenbaugh, N.S., Giorgi, F., Pal, J.S., 2008. Climate change hotspots in the United States. Geophys. Res. Lett. 35 https://doi.org/10.1029/2008GL035075.

Eyring, V., Bony, S., Meehl, G.A., Senior, C.A., Stevens, B., Stouffer, R.J., Taylor, K.E., 2016. Overview of the coupled model Intercomparison Project phase 6 (CMIP6) experimental design and organization. Geosci. Model Dev. (GMD) 9, 1937–1958. https://doi.org/10.5194/gmd-9-1937-2016.

Falcão, A.X., Stolfi, J., De Alencar Lotufo, R., 2004. The image foresting transform: theory, algorithms, and applications. IEEE Trans. Pattern Anal. Mach. Intell. 26, 19–29. https://doi.org/10.1109/TPAMI.2004.1261076.

Fischer, E.M., Knutti, R., 2013. Robust projections of combined humidity and temperature extremes. Nat. Clim. Change 3, 126–130. https://doi.org/10.1038/nclimate1682.

Giorgi, F., 2006. Climate change hot-spots. Geophys. Res. Lett. 33, L08707 https://doi.org/10.1029/2006GL025734.

Goswami, B.N., Venugopal, V., Sengupta, D., Madhusoodanan, M.S., Xavier, P.K., 2006. Increasing trend of extreme rain events over India in a warming environment. Science 84 314, 1442–1445. https://doi.org/10.1126/science.1132027.

Gu, H., Yu, Z., Wang, J., Ju, Q., Yang, C., Fan, C., 2014. Climate change hotspots identification in China through the CMIP5 global climate model ensemble. Adv. Meteorol. 1–10. https://doi.org/10.1155/2014/963196, 2014.

Gupta, H.V., Sorooshian, S., Yapo, P.O., 1999. Status of automatic calibration for hydrologic models: comparison with multilevel expert calibration. J. Hydrol. Eng. 4, 135–143. https://doi.org/10.1061/(asce)1084-0699.

Hawkins, E., Sutton, R., 2012. Time of emergence of climate signals. Geophys. Res. Lett. 39 https://doi.org/10.1029/2011GL050087.

Hendry, A., Haigh, I., Nicholls, R., Winter, H., Neal, R., Wahl, T., Joly-Laugel, A., Darby, S., 2019. Assessing the characteristics and drivers of compound flooding events around the UK coast. Hydrol. Earth Syst. Sci. Discuss. 1–52. https://doi.org/10.5194/hess-2018-632.

Kandlikar, M., Risbey, J., Dessai, S., 2005. Representing and communicating deep uncertainty in climate-change assessments. Compt. Rendus Geosci. 337, 443–455. https://doi.org/10.1016/j.crte.2004.10.010.

Knutti, R., Sedláček, J., Sanderson, B.M., Lorenz, R., Fischer, E.M., Eyring, V., 2017. A climate model projection weighting scheme accounting for performance and interdependence. Geophys. Res. Lett. 44, 1909–1918. https://doi.org/10.1002/2016GL072012.

Lau, N.-C., Nath, M.J., 2014. Model simulation and projection of European heat waves in present-day and future climates. J. Clim. 27, 3713–3730. https://doi.org/10.1175/JCLI-D-13-00284.1.

Lau, N.-C., Nath, M.J., 2012. A model study of heat waves over north America: meteorological aspects and projections for the twenty-first century. J. Clim. 25, 4761–4784. https://doi.org/10.1175/JCLI-D-11-00575.1.

Leonard, M., Westra, S., Phatak, A., Lambert, M., van den Hurk, B., McInnes, K., Risbey, J., Schuster, S., Jakob, D., Stafford-Smith, M., 2014. A compound event framework for understanding extreme impacts. Wiley Interdiscip. Rev. Clim. Chang. 5, 113–128. https://doi.org/10.1002/wcc.252.

Liu, Z., Anderson, B., Yan, K., Dong, W., Liao, H., Shi, P., 2017. Global and regional changes in exposure to extreme heat and the relative contributions of climate and population change. Sci. Rep. 7 https://doi.org/10.1038/srep43909.

Lu, Y., Hu, H., Li, C., Tian, F., 2018. Increasing compound events of extreme hot and dry days during growing seasons of wheat and maize in China. Sci. Rep. 8, 16700 https://doi.org/10.1038/s41598-018-34215-y.

Mazdiyasni, O., AghaKouchak, A., Davis, S.J., Madadgar, S., Mehran, A., Ragno, E., Sadegh, M., Sengupta, A., Ghosh, S., Dhanya, C.T., Niknejad, M., 2017. Increasing probability of mortality during Indian heat waves. Sci. Adv. 3, e1700066 https://doi.org/10.1126/sciadv.1700066.

Mishra, V., Bhatia, U., Tiwari, A.D., 2020. Bias-corrected climate projections for South Asia from coupled model Intercomparison project-6. Sci. Data 7, 338. https://doi.org/10.1038/s41597-020-00681-1.

Moftakhari, H.R., Salvadori, G., AghaKouchak, A., Sanders, B.F., Matthew, R.A., 2017. Compounding effects of sea level rise and fluvial flooding. Proc. Natl. Acad. Sci. U.S. A. 114, 9785–9790. https://doi.org/10.1073/pnas.1620325114.

Mujumdar, P.P., Ghosh, S., 2008. Modeling GCM and scenario uncertainty using a possibilistic approach: application to the Mahanadi River, India. Water Resour. Res. 44 https://doi.org/10.1029/2007WR006137.

Mukherjee, S., Aadhar, S., Stone, D., Mishra, V., 2018. Increase in extreme precipitation events under anthropogenic warming in India. Weather Clim. Extrem. 20, 45–53. https://doi.org/10.1016/j.wace.2018.03.005.

Muthuvel, D., Mahesha, A., 2021. Spatiotemporal analysis of compound agrometeorological drought and hot events in India using a standardized index. J. Hydrol. Eng. 26 https://doi.org/10.1061/(asce)he.1943-5584.0002101.

Narula, P., Sarkar, K., Azad, S., 2018. A functional evaluation of the spatiotemporal patterns of temperature change in India. Int. J. Climatol. 38, 264–271. https://doi.org/10.1002/joc.5174.

Nash, J.E., Sutcliffe, J.V., 1970. River flow forecasting through conceptual models part I — a discussion of principles. J. Hydrol. 10, 282–290. https://doi.org/10.1016/0022-1694(70)90255-6.

Nikumbh, A.C., Chakraborty, A., Bhat, G.S., 2019. Recent spatial aggregation tendency of rainfall extremes over India. Sci. Rep. 9, 1–7. https://doi.org/10.1038/s41598-019-46719-2.

Ning, G., Luo, M., Zhang, W., Liu, Z., Wang, S., Gao, T., 2022. Rising risks of compound extreme heat-precipitation events in China. Int. J. Climatol. 42, 5785–5795. https://doi.org/10.1002/joc.7561.

Pai, D.S., Sridhar, L., Rajeevan, M., Sreejith, O.P., Satbhai, N.S., Mukhopadyay, B., 2014. Development of a new high spatial resolution (0.25° × 0.25°) Long Period (1901-2010) daily gridded rainfall data set over India and its comparison with existing data sets over the region. Mausam 65, 1–18.

Pradhan, P., Shrestha, S., Sundaram, S.M., Virdis, S.G.P., 2021. Evaluation of the CMIP5 general circulation models for simulating the precipitation and temperature of the Koshi River Basin in Nepal. J. Water Clim. Chang. 12, 3282–3296. https://doi.org/10.2166/wcc.2021.124.

Raju, K.S., Kumar, D.N., 2014. Ranking of global climate models for India using multicriterion analysis. Clim. Res. 60, 103–117. https://doi.org/10.3354/cr01222.
Raymond, C., Horton, R.M., Zscheischler, J., Martius, O., AghaKouchak, A., Balch, J., Bowen, S.G., Camargo, S.J., Hess, J., Kornhuber, K., Oppenheimer, M., Ruane, A.C., Wahl, T., White, K., 2020. Understanding and managing connected extreme events. Nat. Clim. Change 10, 611–621. https://doi.org/10.1038/s41558-020-0790-4.
Sadegh, M., Moftakhari, H., Gupta, H.V., Ragno, E., Mazdiyasni, O., Sanders, B., Matthew, R., AghaKouchak, A., 2018. Multihazard scenarios for analysis of compound extreme events. Geophys. Res. Lett. 45, 5470–5480. https://doi.org/10.1029/2018GL077317.
Saha, U., Sateesh, M., 2022. Rainfall extremes on the rise: observations during 1951–2020 and bias-corrected CMIP6 projections for near- and late 21st century over Indian landmass. J. Hydrol. 608 https://doi.org/10.1016/j.jhydrol.2022.127682.
Sarkar, S., Maity, R., 2022. Future characteristics of extreme precipitation indicate the dominance of frequency over intensity: a multi-model assessment from CMIP6 across India. J. Geophys. Res. Atmos. 127 https://doi.org/10.1029/2021JD035539.
Seneviratne, S., Nicholls, N., Easterling, D., Goodess, C., Kanae, S., Kossin, J., Luo, Y., Marengo, J., McInnes, K., Rahimi, M., 2012. Managing the Risks of Extreme Events and Disasters to Advance Climate Change Adaptation a Special Report of Working Groups I and II of the Intergovernmental Panel on Climate Change (IPCC).
Sharma, S., Mujumdar, P., 2017. Increasing frequency and spatial extent of concurrent meteorological droughts and heatwaves in India. Sci. Rep. 7, 15582 https://doi.org/10.1038/s41598-017-15896-3.
Sherbinin, A., 2014. Climate change hotspots mapping: what have we learned? Clim. Change 123, 23–37.
Singh, S., Mall, R.K., Singh, N., 2021. Changing spatio-temporal trends of heat wave and severe heat wave events over India: an emerging health hazard. Int. J. Climatol. 41 https://doi.org/10.1002/joc.6814.
Srinivasa Raju, K., Sonali, P., Nagesh Kumar, D., 2017. Ranking of CMIP5-based global climate models for India using compromise programming. Theor. Appl. Climatol. 128, 563–574. https://doi.org/10.1007/s00704-015-1721-6.
Srivastava, A.K., Rajeevan, M., Kshirsagar, S.R., 2009. Development of a high resolution daily gridded temperature data set (1969-2005) for the Indian region. Atmos. Sci. Lett. n/a-n/a. https://doi.org/10.1002/asl.232.
Suman, M., Maity, R., 2020. Southward shift of precipitation extremes over south Asia: evidences from CORDEX data. Sci. Rep. 10, 6452. https://doi.org/10.1038/s41598-020-63571-x.
Tencer, B., Bettolli, M., Rusticucci, M., 2016. Compound temperature and precipitation extreme events in southern South America: associated atmospheric circulation, and simulations by a multi-RCM ensemble. Clim. Res. 68, 183–199. https://doi.org/10.3354/cr01396.
Teng, J., Vaze, J., Chiew, F.H.S., Wang, B., Perraud, J.-M., 2012. Estimating the relative uncertainties sourced from GCMs and hydrological models in modeling climate change impact on runoff. J. Hydrometeorol. 13, 122–139. https://doi.org/10.1175/JHM-D-11-058.1.
Tilloy, A., Malamud, B., Joly-Laugel, A., 2021. A methodology for the spatiotemporal identification of compound hazards: wind and precipitation extremes in great britain (1979–2019). Earth Syst. Dyn. Discuss. 1–45 https://doi.org/10.5194/esd-2021-52.
Van Den Hurk, B., Van Meijgaard, E., De Valk, P., Van Heeringen, K.J., Gooijer, J., 2015. Analysis of a compounding surge and precipitation event in The Netherlands. Environ. Res. Lett. 10 https://doi.org/10.1088/1748-9326/10/3/035001.
Vishwakarma, V., Pattnaik, S., 2022. Role of large-scale and microphysical precipitation efficiency on rainfall characteristics of tropical cyclones over the Bay of Bengal. Nat. Hazards 114, 1585–1608. https://doi.org/10.1007/s11069-022-05439-z.
Wahl, T., Jain, S., Bender, J., Meyers, S.D., Luther, M.E., 2015. Increasing risk of compound flooding from storm surge and rainfall for major US cities. Nat. Clim. Change 5, 1093–1097. https://doi.org/10.1038/nclimate2736.
Weber, T., Bowyer, P., Rechid, D., Pfeifer, S., Raffaele, F., Remedio, A.R., Teichmann, C., Jacob, D., 2020. Analysis of compound climate extremes and exposed population in africa under two different emission scenarios. Earth's Future 8. https://doi.org/10.1029/2019EF001473.
Williams, J.W., Jackson, S.T., Kutzbach, J.E., 2007. Projected distributions of novel and disappearing climates by 2100 AD. Proc. Natl. Acad. Sci. U.S.A. 104, 5738–5742. https://doi.org/10.1073/pnas.0606292104.
Yu, H., Lu, N., Fu, B., Zhang, L., Wang, M., Tian, H., 2022. Hotspots, co-occurrence, and shifts of compound and cascading extreme climate events in Eurasian drylands. Environ. Int. 169 https://doi.org/10.1016/j.envint.2022.107509.
Zscheischler, J., Martius, O., Westra, S., Bevacqua, E., Raymond, C., Horton, R.M., van den Hurk, B., AghaKouchak, A., Jézéquel, A., Mahecha, M.D., Maraun, D., Ramos, A. M., Ridder, N.N., Thiery, W., Vignotto, E., 2020. A typology of compound weather and climate events. Nat. Rev. Earth Environ. 1, 333–347. https://doi.org/10.1038/s43017-020-0060-z.
Zscheischler, J., Seneviratne, S.I., 2017. Dependence of drivers affects risks associated with compound events. Sci. Adv. 3, e1700263 https://doi.org/10.1126/sciadv.1700263.
Zscheischler, J., Westra, S., van den Hurk, B.J.J.M., Seneviratne, S.I., Ward, P.J., Pitman, A., AghaKouchak, A., Bresch, D.N., Leonard, M., Wahl, T., Zhang, X., 2018. Future climate risk from compound events. Nat. Clim. Change 8, 469–477. https://doi.org/10.1038/s41558-018-0156-3.

Update

Environmental Research

Volume 236, Issue P2, 1 November 2023, Page

DOI: https://doi.org/10.1016/j.envres.2023.116840

Environmental Research 236 (2023) 116840

Contents lists available at ScienceDirect

Environmental Research

journal homepage: www.elsevier.com/locate/envres

Corrigendum

Corrigendum to spatio-temporal compounding of connected extreme events: Projection and hotspot identification Environ. Res. **235** (2023) 116615

Manikanta Velpuri, Jew Das *, N.V. Umamahesh

National Institute of Technology, Warangal, India

We, the authors of this manuscript, regret to inform that we noticed that the legend in **Fig. 5** and **Figs. S8 to S12** were mistakenly inverted in our published manuscript. Unfortunately, there was an inadvertent mistake in the drawing of these legends, resulting in an inversion that does not accurately represent the intended information.

Specifically, the original intention was to have the legends inverted, but they were mistakenly drawn in the opposite manner. We sincerely apologize for this oversight, and we understand the importance of ensuring accurate representation of the data.

To clarify, we have provided the corrected legends of **Fig. 5** and **Figs. S8 to S12** (in supplementary information). We have attached the corrected versions of **Fig. 5** and **Figs. S8 to S12** for your convenience. The figures themselves remain unchanged, and only the legends were corrected.

We want to emphasize that this correction does not impact the validity of our research findings, nor does it affect the interpretation of the results or any other part of the manuscript. The corrections are purely intended to provide readers with the correct information for a comprehensive understanding of the results. We assure you that the corrected legends align with the intended message conveyed by the figures.

We would like to apologize for any inconvenience caused.

DOI of original article: https://doi.org/10.1016/j.envres.2023.116615.

* Corresponding author.
E-mail address: jewdas05@gmail.com (J. Das).

https://doi.org/10.1016/j.envres.2023.116840

Available online 9 August 2023

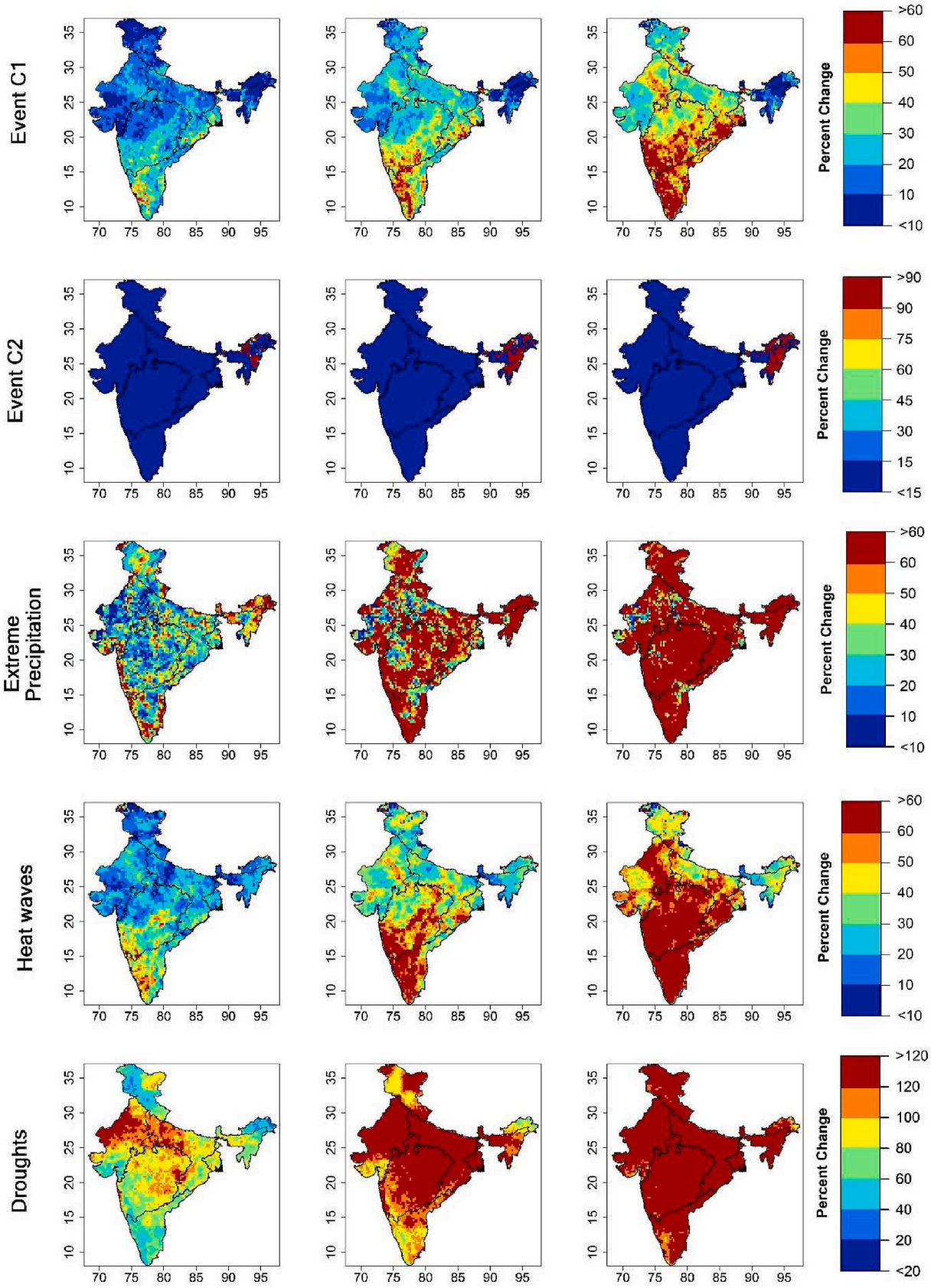

Fig. 5. The percentage change of mean duration (i.e., mean of all durations during 1977–2016) of extreme events in case of small-scale spatial compounding. The temporal compounding for 1-, 2-, and 3-days is presented (column-wise arrangement) in terms of percentage change with respect to the 0-day temporal compounding.

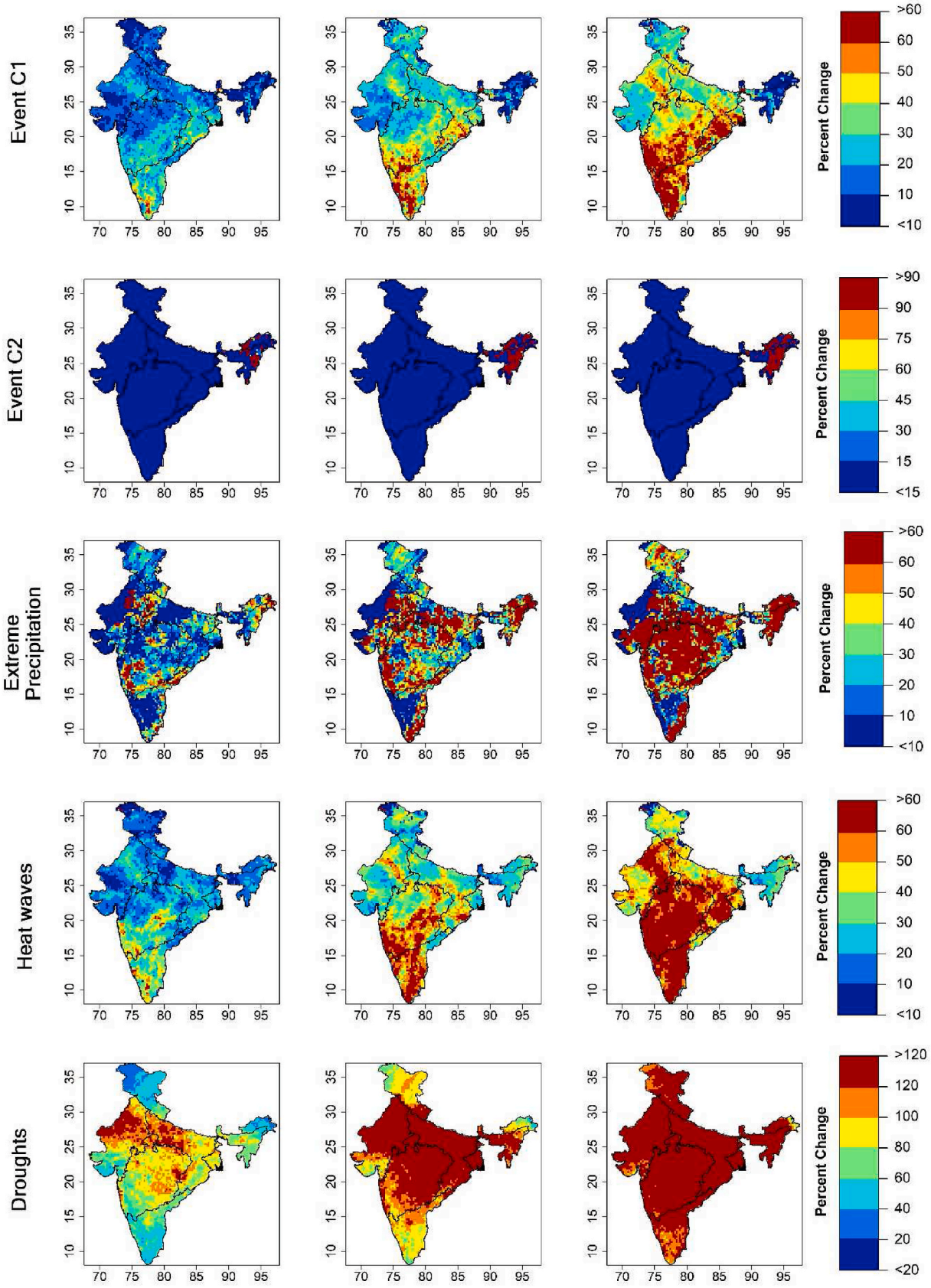

Fig. S8. The percentage change of mean duration (i.e., mean of all durations during 1977–2016) of extreme events in case of medium-scale spatial compounding. The temporal compounding for 1-, 2-, and 3-days is presented (column-wise arrangement) in terms of percentage change with respect to the 0-day temporal compounding.

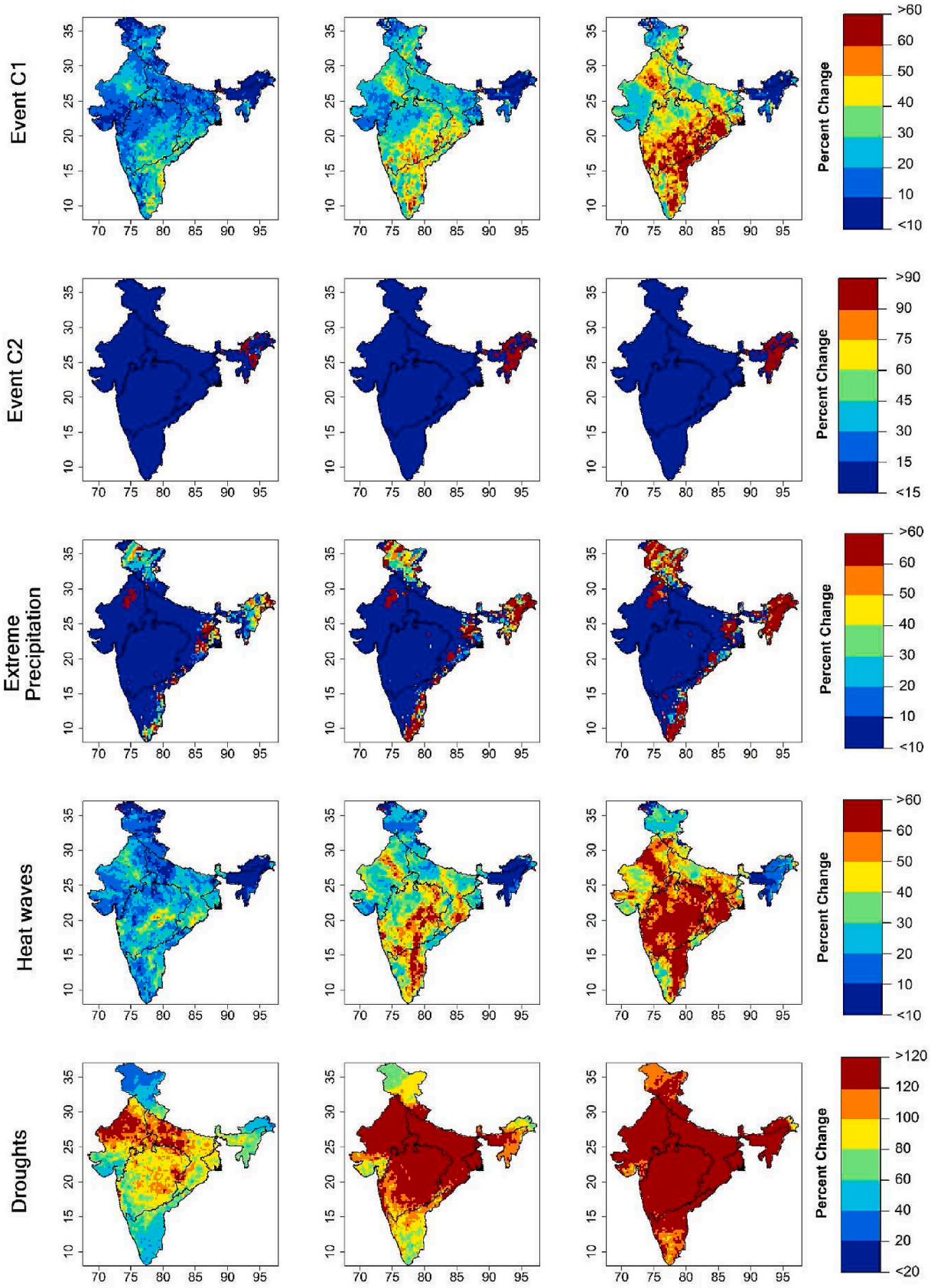

Fig. S9. The percentage change of mean duration (i.e., mean of all durations during 1977–2016) of extreme events in case of large-scale spatial compounding. The temporal compounding for 1-, 2-, and 3-days is presented (column-wise arrangement) in terms of percentage change with respect to the 0-day temporal compounding.

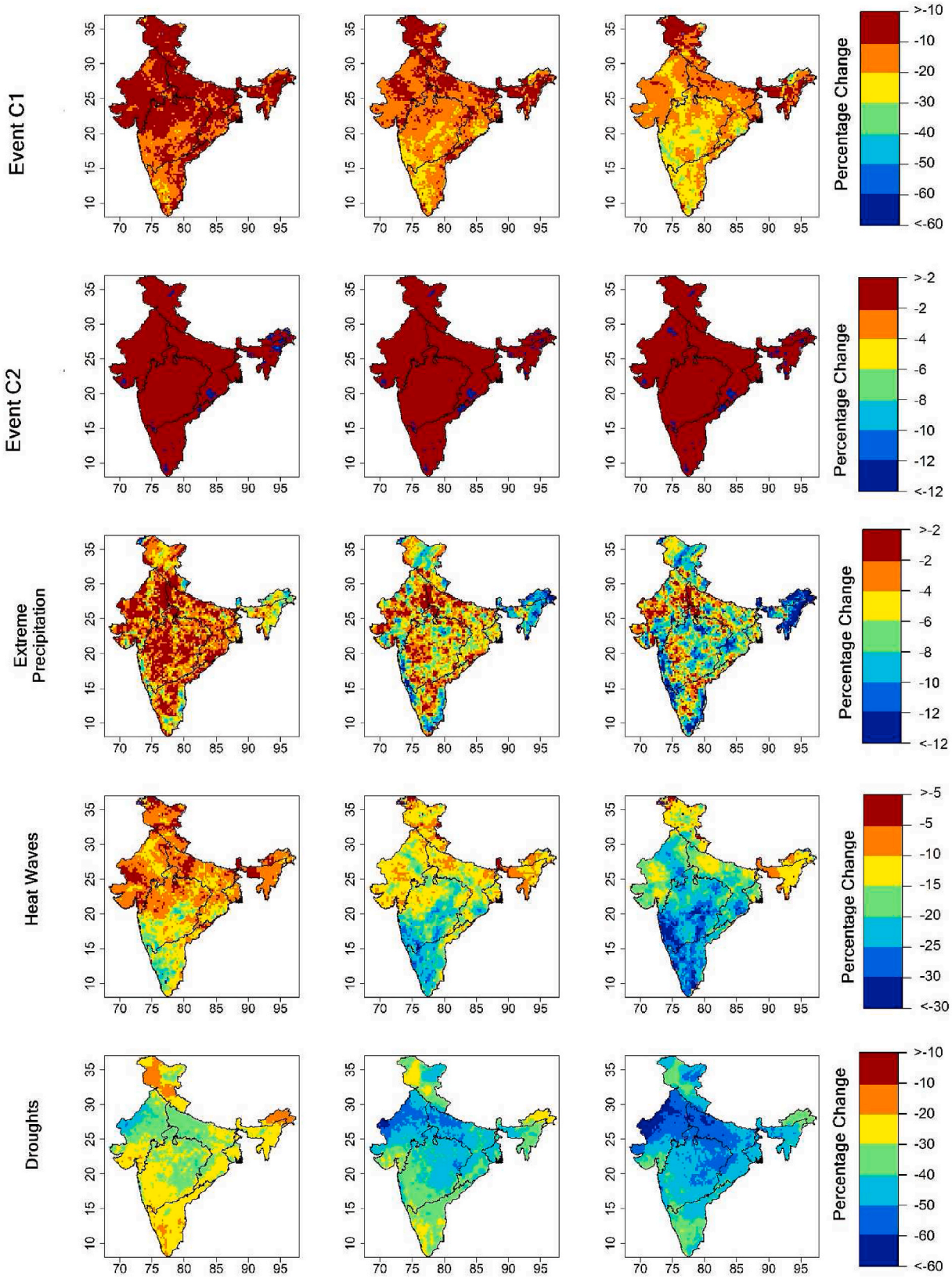

Fig. S10. The percentage change of mean occurrence (i.e., mean of all events during 1977–2016) of extreme events in case of small-scale spatial compounding. The temporal compounding for 1-, 2-, and 3-days is presented (column-wise arrangement) in terms of percentage change with respect to the 0-day temporal compounding.

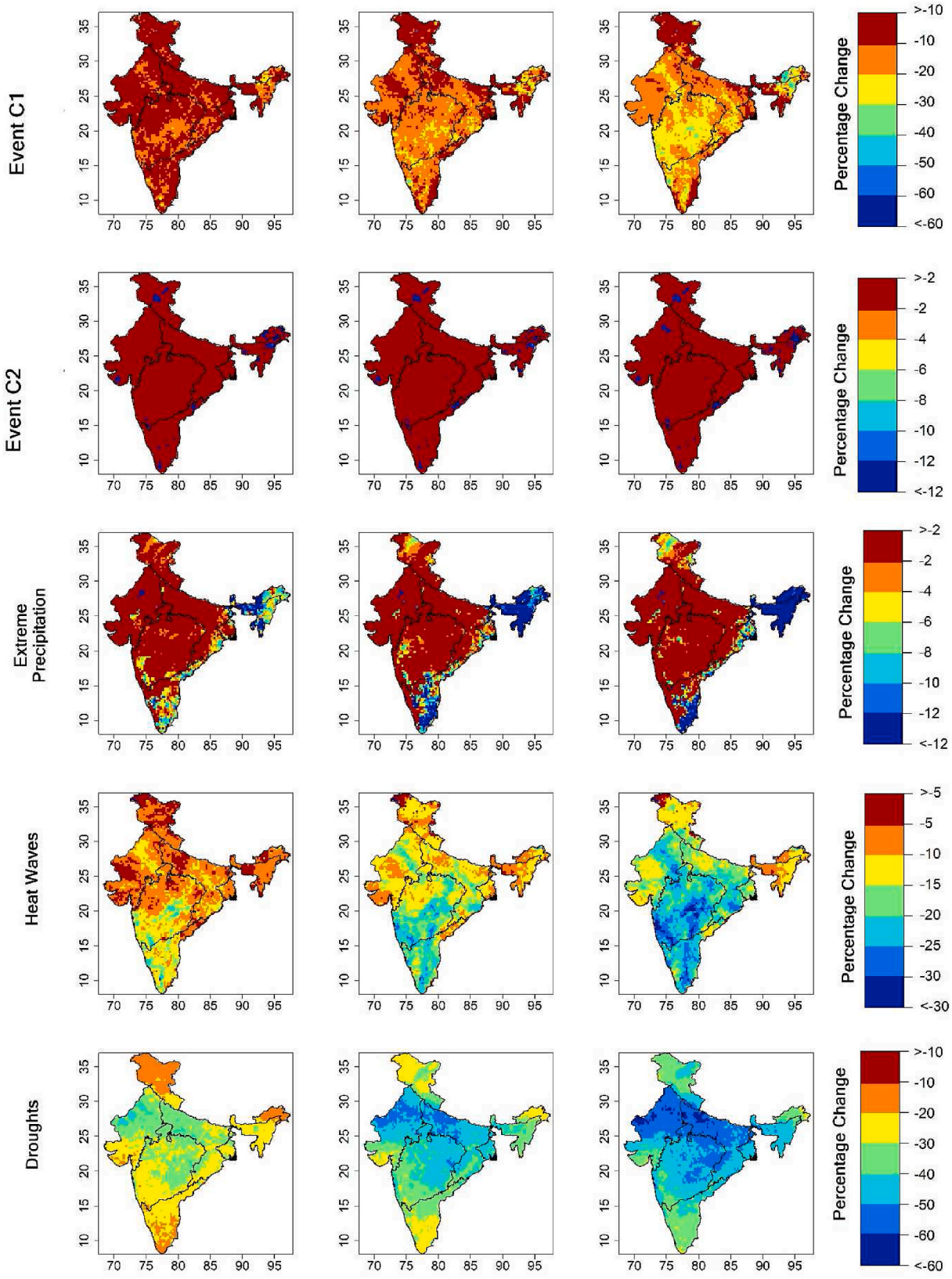

Fig. S11. The percentage change of mean occurrence (i.e., mean of all events during 1977–2016) of extreme events in case of medium-scale spatial compounding. The temporal compounding for 1-, 2-, and 3-days is presented (column-wise arrangement) in terms of percentage change with respect to the 0-day temporal compounding.

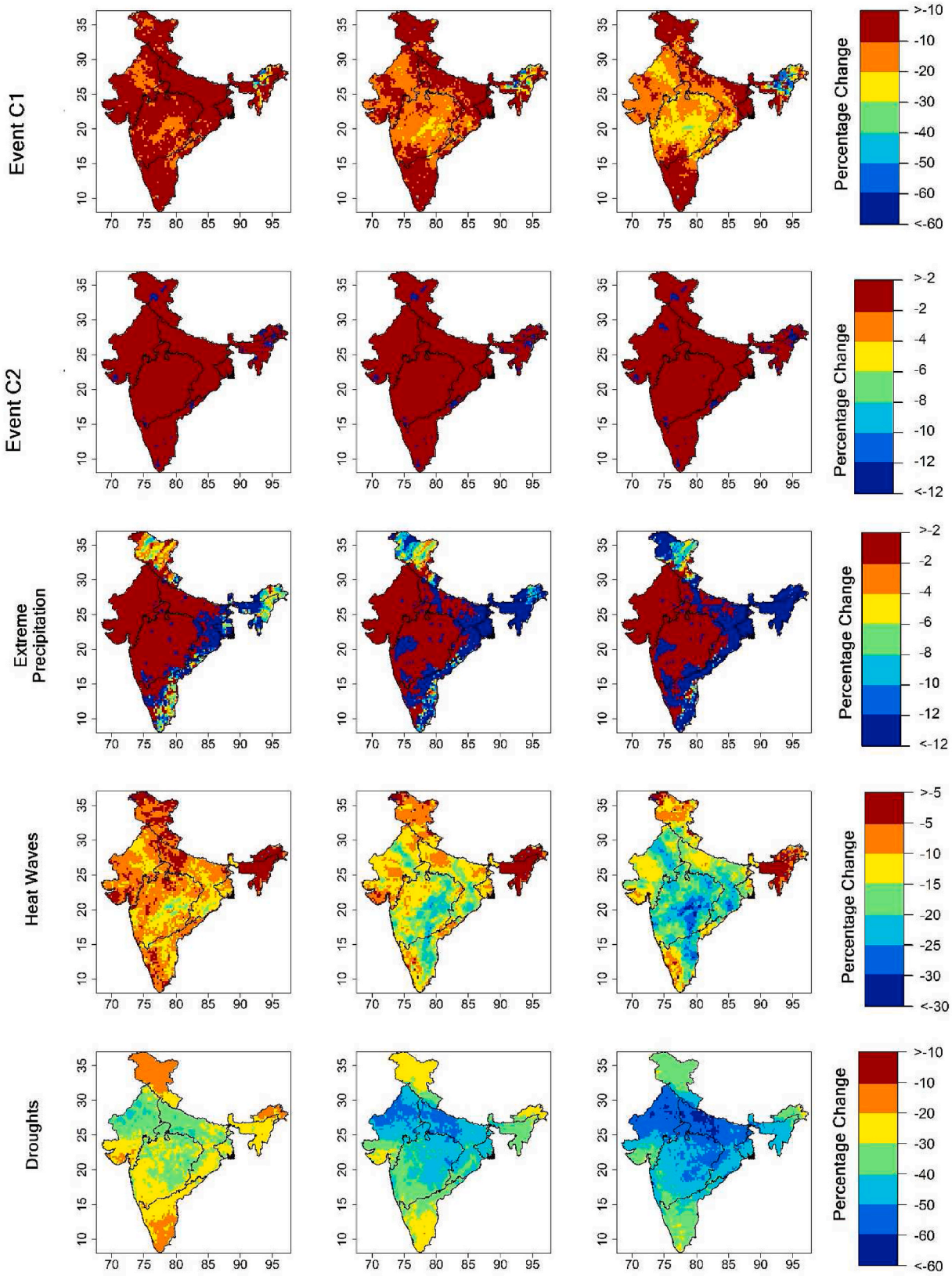

Fig. S12. The percentage change of mean occurrence (i.e., mean of all events during 1977–2016) of extreme events in case of large-scale spatial compounding. The temporal compounding for 1-, 2-, and 3-days is presented (column-wise arrangement) in terms of percentage change with respect to the 0-day temporal compounding.